Liquid helium on a surface: Ground state, excitations, condensate fraction, and impurity potential

E. Krotscheck
*Max-Planck Institut für Kernphysik, D-6900 Heidelberg, West Germany**
and Department of Physics, Texas A&M University, College Station, Texas 77843-4242
(Received 20 September 1984; revised manuscript received 11 February 1985)

We study the structure of films of ^{4}He atoms adsorbed to a plane substrate. The ground state is described within a variational model developed earlier [E. Krotscheck, G.-X. Qian, and W. Kohn, Phys Rev. B **31**, 4245 (1985)]. Euler-Lagrange equations are solved for the one-body and two-body correlations for three different models of the ^{4}He-substrate interaction. The one-body density shows structure indicating the formation of layers of one, two, three, ... atoms above the substrate. The solution of the Euler-Lagrange equation also provides the dispersion relation and spatial shape of collective excitations in the system. The results of the ground-state optimization are used to calculate the condensate fraction (i.e., the number of particles with zero momentum parallel to the surface) and the binding energy of a ^{3}He impurity.

I. INTRODUCTION

Microscopic calculations of properties of strongly interacting quantum systems often start from a variational *ansatz* for the ground-state wave function of the Feenberg form,[1,2]

$$|\Psi_0\rangle = \exp\left[\frac{1}{2}\sum_{i=1}^{A} u_1(\mathbf{r}_i) + \frac{1}{2}\sum_{\substack{i,j=1\\ i<j}}^{A} u_2(\mathbf{r}_i,\mathbf{r}_j) + \cdots\right]|\Phi_0\rangle \ , \tag{1.1}$$

where $|\Phi_0\rangle$ is an appropriately chosen model wave function reflecting the symmetries and the statistics of the system under consideration. The $u_n(\mathbf{r}_1,\mathbf{r}_2,\ldots,\mathbf{r}_n)$ are n-body correlation factors; they vanish whenever one or more of the particles is moved far away from the rest. The *ansatz* (1.1) is especially suitable for Bose systems, where the model ground state $|\Phi_0\rangle$ can be chosen to be 1. In that case, the form (1.1) is, in principle, an exact representation of the ground state.

The wave function (1.1) has been applied mostly to studies of homogeneous quantum liquids. For liquid ^{4}He, the subject of this paper, the results are adequately reviewed in Refs. 3. The translational invariance of the system in all directions simplifies the analytic structure of the correlation functions substantially: $u_1(\mathbf{r})$ is a constant and may be chosen to be zero. $u_2(\mathbf{r}_i,\mathbf{r}_j)$ depends only on the distance $r_{ij} = |\mathbf{r}_i - \mathbf{r}_j|$ between the two particles. It is therefore easy to perform partial summations of the energy expectation value,

$$H_{00} = \frac{\langle\Psi_0|H|\Psi_0\rangle}{\langle\Psi_0|\Psi_0\rangle} \ , \tag{1.2}$$

in a diagrammatic cluster expansion.[2] These may then be compared with direct Monte Carlo integrations[4] of the energy H_{00}. It is also possible to optimize the pair correlations by the variational principle,[5,6]

$$\frac{\delta H_{00}}{\delta u_2}(r) = 0 \ . \tag{1.3}$$

Of course, the Euler-Lagrange (EL) equation (1.3) is not guaranteed to give the correct answer for the "best" two-body correlations if it is applied to an approximate energy expectation value. One of the important steps in the development of the variational theory was to show[2] that optimizing the hypernetted-chain (HNC) approximation for H_{00} preserves the important properties of the full variational principle. Moreover, when used with the Euler-Lagrange equation (1.3), the HNC approximation exhibits the known physical instabilities of the system: at low densities against droplet formation,[7] and at high densities against the formation of a quantum solid.[8] The most important consequence of this property of the theory for our application is that the HNC/EL theory has built-in signs which tell us whether a given number of particles fills this volume uniformly, or only partly.

There are also a number of studies of inhomogeneous systems (in particular, the free surface of liquid ^{4}He) using the variational wave function (1.1). Worth mentioning are the works of Woo and collaborators,[9,10] Chang and Cohen,[11] and more recently, Saarela *et al.*[12] Among these, the pioneering work of Ref. 9 gave the best result for a long time.

In an inhomogeneous system, the two-body correlation factor $u_2(\mathbf{r}_i,\mathbf{r}_j)$ obtained from the Euler-Lagrange equation (1.3) depends on more than the distance between the two particles. For the problem of a plane surface considered here and in Ref. 1 (hereafter called paper I), $u_2(\mathbf{r}_i,\mathbf{r}_j)$ depends on both the distances of each individual particle from the surface and on the distance between the two particles parallel to the surface. This causes some numerical difficulties, and for a long time it was believed that the HNC/EL problem of an inhomogeneous system was overly difficult to be carried out numerically. In I, we have shown how the HNC/EL problem can be solved in an inhomogeneous system with a reasonable numerical

effort. In particular, it is hardly more involved to solve the full optimization problem (1.3) than it is to solve just the HNC equations. But in addition to the ground-state properties, the solution of the HNC/EL problem also provides the dispersion relations and the wave forms of collective excitations (Ref. 13, paper II).

The present paper reports applications of the theory developed in I and II to a physically different case, and presents some extensions of that theory. In I, we have considered free ^{4}He films which are translationally invariant in two directions (say, x and y) and have a symmetric density profile in the z direction. For sufficiently thick films, the theory of I provides a microscopic picture of the free surface of ^{4}He. Here, we again consider systems with translational invariance in the x-y plane, but the helium liquid is in a z-dependent substrate potential $U_{\rm sub}(z)$ which models the adhesion force between ^{4}He atoms and a substrate. The density profiles were quite smooth in the case of a free surface; we will see that the combination of the geometrical restrictions acting on the helium atoms and the compression of the liquid due to the attractive substrate potential induce a layer structure in the density. The layer structure of the one-body density mentioned above is testimonial to the power of the unconstrained HNC/EL theory. One need not rely on "educated guesses" for the one-body density or the one-body correlation factor $u_1(\mathbf{r})$.

The basic equations of the theory are reviewed in Sec. II. Results for the ground-state energetics and the one-body density are presented in Sec. III. Sections IV, V, and VI turn to two simple extensions of the theory.

Section IV discusses the spectrum and wave forms of the collective excitations. Section V studies the density matrix, which is of interest for finite-temperature extensions of the theory[14,15] and possibly experimentally accessible through neutron scattering experiments.[16] The theoretical methods have been foreseen some time ago by Ristig and Clark *et al.*[17] The generalization of that work to the inhomogeneous case is essentially straightforward, but it illuminates the diagrammatic structure of the cluster expansions better than the theory for the bulk system. Along with the derivation, we will formulate a new consistency constraint for approximations for the density matrix. The theory of the density matrix is not only of formal and physical interest; it also has the amusing property that the HNC theory for that quantity[18] sums precisely the wrong classes of diagrams. The only quantity that can be calculated reliably is the condensate fraction, and we will present results for this quantity.

Section IV investigates the binding of a single ^{3}He atom to the surface of ^{4}He. For all models under consideration, we find two discrete bound states of the ^{3}He atom, the low-lying localized in the surface of the ^{4}He layer, and another close to the substrate. When the film is thick enough, or in a strong substrate potential, a third bound state appears; it corresponds to the state of a particle confined in a box between the substrate and the surface of the film. This state is the one which tends to the state of a single ^{3}He atom in ^{4}He in the bulk limit. The final section, VII, gives an overview of our results.

II. OPTIMIZATION OF THE GROUND STATE

Let us now specify the model under consideration and review briefly the techniques used in solving the problem. The reader is directed to I for details of the derivations. We consider a system of interacting particles in an external one-body potential, i.e., the Hamiltonian of the system is of the form

$$H=-\frac{\hbar^2}{2m}\sum_{i=1}^{A}\nabla_i^2+\sum_{i=1}^{A}U_{\rm sub}(\mathbf{r}_i)+\sum_{\substack{i,j=1\\ i<j}}^{A}v(|\mathbf{r}_i-\mathbf{r}_j|)\,. \tag{2.1}$$

(In practical applications, we will consider an external field which depends on only one coordinate, say z. However, this simplification is not used in the formal developments.) The wave function of the system is assumed to be of the Feenberg form (1.1); we neglect all but the one- and two-body components, $u_1(\mathbf{r})$ and $u_2(\mathbf{r}_1,\mathbf{r}_2)$. The ground-state energy can then be written as

$$H_{00}=(\Delta E_1)+(\Delta E_2)\,, \tag{2.2}$$

with

$$(\Delta E_1)=\int d^3r\,\rho_1(\mathbf{r})\left[U_{\rm sub}(\mathbf{r})+\frac{\hbar^2}{8m}|\nabla\ln\rho_1(\mathbf{r})|^2\right], \tag{2.3}$$

and

$$(\Delta E_2)=\tfrac{1}{2}\int d^3r_1\int d^3r_2\,\rho_2(\mathbf{r}_1,\mathbf{r}_2)v_{\rm JF}(\mathbf{r}_1,\mathbf{r}_2)\,. \tag{2.4}$$

$v_{\rm JF}(\mathbf{r}_1,\mathbf{r}_2)$ is the generalized Jackson-Feenberg interaction,

$$v_{\rm JF}(\mathbf{r}_1,\mathbf{r}_2)=v(|\mathbf{r}_1-\mathbf{r}_2|)-\frac{\hbar^2}{8m}\left[\frac{1}{\rho_1(\mathbf{r}_1)}\nabla_{\mathbf{r}_1}\rho_1(\mathbf{r}_1)\cdot\nabla_{\mathbf{r}_1}+\frac{1}{\rho_1(\mathbf{r}_2)}\nabla_{\mathbf{r}_2}\rho_1(\mathbf{r}_2)\cdot\nabla_{\mathbf{r}_2}\right]u_2(\mathbf{r}_1,\mathbf{r}_2)\,, \tag{2.5}$$

and $\rho_1(\mathbf{r})$ and $\rho_2(\mathbf{r}_1,\mathbf{r}_2)$ are the one- and two-body densities. The representation of the ground-state energy (2.3)—(2.5) is derived by eliminating the one-body correlation factor $u_1(\mathbf{r})$ in favor of the one-body density using the first Born-Green-Yvon equation

$$\nabla\rho_1(\mathbf{r}_1)=\rho_1(\mathbf{r}_1)\nabla u_1(\mathbf{r}_1)+\int d^3r_2\,\rho_2(\mathbf{r}_1,\mathbf{r}_2)\nabla_{\mathbf{r}_1}u_2(\mathbf{r}_1,\mathbf{r}_2)\,. \tag{2.6}$$

The relation between the two-body density and the two-body correlation factor is provided by the hypernetted-chain equations:

$$g(\mathbf{r}_1,\mathbf{r}_2)=\frac{\rho_2(\mathbf{r}_1,\mathbf{r}_2)}{\rho_1(\mathbf{r}_1)\rho_1(\mathbf{r}_2)}$$

$$=\exp[u_2(\mathbf{r}_1,\mathbf{r}_2)+N(\mathbf{r}_1,\mathbf{r}_2)+E(\mathbf{r}_1,\mathbf{r}_2)]-1\,, \tag{2.7a}$$

$$X(\mathbf{r}_1,\mathbf{r}_2)=g(\mathbf{r}_1,\mathbf{r}_2)-1-N(\mathbf{r}_1,\mathbf{r}_2)\ , \tag{2.7b}$$

$$N(\mathbf{r}_1,\mathbf{r}_2)=\int d^3r_3\rho_1(\mathbf{r}_3)[g(\mathbf{r}_1,\mathbf{r}_3)-1]X(\mathbf{r}_3,\mathbf{r}_2)\ . \tag{2.7c}$$

Equations (2.7) form a closed set of equations for calculating the pair distribution function $g(\mathbf{r}_1,\mathbf{r}_2)$ from a given two-body correlation factor $u_2(\mathbf{r}_1,\mathbf{r}_2)$ and a given set of "elementary diagrams" $E(\mathbf{r}_1,\mathbf{r}_2)$. The simplest choice is the "HNC approximation" $E(\mathbf{r}_1,\mathbf{r}_2)=0$; we shall use it throughout our paper. This approximation introduces numerical uncertainites of a similar size to those caused by the omission of three-body correlations. Given the two-body Feenberg choice of the wave function, the HNC approximation is the only approximation used in the ground-state part of our paper.

Using the HNC equations, the Euler-Lagrange equations can be put into a quite compact and plausible form. Since we have already eliminated $u_1(\mathbf{r})$, we consider $\rho_1(\mathbf{r})$ as the independent one-body function in minimizing the energy at constant particle number. The corresponding EL equation has the form of a Hartree equation for the square root of the one-body density:

$$-\frac{\hbar^2}{2m}\nabla^2[\rho_1(\mathbf{r})]^{1/2}+[U_{\text{sub}}(\mathbf{r})+V_H(\mathbf{r})][\rho_1(\mathbf{r})]^{1/2}=\mu[\rho_1(\mathbf{r})]^{1/2}\ , \tag{2.8}$$

where μ is the chemical potential, and $V_H(\mathbf{r})$ a generalized Hartree potential,

$$V_H(\mathbf{r})=\frac{\delta(\Delta E_2)}{\delta\rho_1(\mathbf{r})}\ . \tag{2.9}$$

Working formulas for $V_H(\mathbf{r})$ have been derived in I:

$$V_H(\mathbf{r})=V_H^{(1)}(\mathbf{r})+V_H^{(2)}(\mathbf{r})\ , \tag{2.10a}$$

with

$$V_H^{(1)}(\mathbf{r}_1)=\int d_2^3\rho_1(\mathbf{r}_2)\left[V_{\text{p-h}}(\mathbf{r}_1,\mathbf{r}_2)-\frac{\hbar^2}{8m}[g(\mathbf{r}_1,\mathbf{r}_2)-1]\left[\frac{1}{\rho_1(\mathbf{r}_1)}\nabla_{\mathbf{r}_1}\rho_1(\mathbf{r}_1)\cdot\nabla_{\mathbf{r}_1}+\frac{1}{\rho_1(\mathbf{r}_2)}\nabla_{\mathbf{r}_2}\rho_1(\mathbf{r}_2)\cdot\nabla_{\mathbf{r}_2}\right]N(\mathbf{r}_1,\mathbf{r}_2)\right.$$
$$\left.+\frac{\hbar^2}{8m}N(\mathbf{r}_1,\mathbf{r}_2)\frac{1}{\rho_1(\mathbf{r}_2)}\nabla_{\mathbf{r}_2}\rho_1(\mathbf{r}_2)\cdot\nabla_{\mathbf{r}_2}X(\mathbf{r}_1,\mathbf{r}_2)\right]\ , \tag{2.10b}$$

and

$$V_H^{(2)}(\mathbf{r}_1)=-\frac{\hbar^2}{16m}\frac{1}{\rho_1(\mathbf{r}_1)}\nabla_{\mathbf{r}_1}\rho_1(\mathbf{r}_1)\cdot\nabla_{\mathbf{r}_1}\int d^3r_2\rho_1(\mathbf{r}_2)[g(\mathbf{r}_1,\mathbf{r}_2)-1]N(\mathbf{r}_1,\mathbf{r}_2)\ . \tag{2.10c}$$

The "particle-hole interaction" $V_{\text{p-h}}(\mathbf{r}_1,\mathbf{r}_2)$ appearing in Eq. (2.10b) will be defined below.

The Euler-Lagrange equation for the two-body correlations can be formulated in various ways. We have chosen in I an "RPA-like" (where RPA denotes the random-phase approximation) formulation, which is well suited for both solving the equations and studying excited states. In that formulation, the sets of "non-nodal diagrams" $X(\mathbf{r}_1,\mathbf{r}_2)$ [cf. Eq. (2.7b)] are related to the particle-hole interaction $V_{\text{p-h}}(\mathbf{r}_1,\mathbf{r}_2)$ through

$$\frac{\hbar^2}{4m}\left[\left[\frac{1}{\rho_1(\mathbf{r}_1)}\nabla_{\mathbf{r}_1}\rho_1(\mathbf{r}_1)\cdot\nabla_{\mathbf{r}_1}+\frac{1}{\rho_1(\mathbf{r}_2)}\nabla_{\mathbf{r}_2}\rho_1(\mathbf{r}_2)\cdot\nabla_{\mathbf{r}_2}\right]X(\mathbf{r}_1,\mathbf{r}_2)-\int d^3r_3\,X(\mathbf{r}_1,\mathbf{r}_3)\nabla_{\mathbf{r}_3}\rho_1(\mathbf{r}_3)\cdot\nabla_{\mathbf{r}_3}X(\mathbf{r}_3,\mathbf{r}_2)\right]=V_{\text{p-h}}(\mathbf{r}_1,\mathbf{r}_2)\ , \tag{2.11a}$$

with

$$V_{\text{p-h}}(\mathbf{r}_1,\mathbf{r}_2)=\frac{\delta^2(\Delta E_2)}{\delta\rho_1(\mathbf{r}_1)\delta\rho_1(\mathbf{r}_2)}\ . \tag{2.11b}$$

In the HNC approximation, the particle-hole interaction $V_{\text{p-h}}(\mathbf{r}_1,\mathbf{r}_2)$ has the form[1]

$$V_{\text{p-h}}(\mathbf{r}_1,\mathbf{r}_2)=g(\mathbf{r}_1,\mathbf{r}_2)v(|\mathbf{r}_1-\mathbf{r}_2|)+\frac{\hbar^2}{2m}\{|\nabla_1[g(\mathbf{r}_1,\mathbf{r}_2)]^{1/2}|^2+|\nabla_2[g(\mathbf{r}_1,\mathbf{r}_2)]^{1/2}|^2\}$$
$$+\frac{\hbar^2}{4m}[g(\mathbf{r}_1,\mathbf{r}_2)-1]\cdot\left[\frac{1}{\rho_1(\mathbf{r}_1)}\nabla_{\mathbf{r}_1}\rho_1(\mathbf{r}_1)\cdot\nabla_{\mathbf{r}_1}+\frac{1}{\rho_1(\mathbf{r}_2)}\nabla_{\mathbf{r}_2}\rho_1(\mathbf{r}_2)\cdot\nabla_{\mathbf{r}_2}\right]N(\mathbf{r}_1,\mathbf{r}_2)$$
$$+\frac{\hbar^2}{4m}\int d^3r_3X(\mathbf{r}_1,\mathbf{r}_3)\nabla_{\mathbf{r}_3}\rho_1(\mathbf{r}_3)\cdot\nabla_{\mathbf{r}_3}X(\mathbf{r}_3,\mathbf{r}_2)\ . \tag{2.11c}$$

Equation (2.11a) is[1] a boson-RPA equation with the single-particle states generated by the one-body Hamiltonian

$$H_1(\mathbf{r})=-\frac{\hbar^2}{2m}\frac{1}{[\rho_1(\mathbf{r})]^{1/2}}\nabla\rho_1(\mathbf{r})\cdot\nabla\frac{1}{[\rho_1(\mathbf{r})]^{1/2}}\ . \tag{2.12}$$

Equations (2.7), (2.10), and (2.11) form a closed set which permits an iterative scheme leading from an initial guess of the pair distribution function to convergence. Details of the procedure may be found in I.

III. STATIC PROPERTIES

We have solved Eqs. (2.10) and (2.11) for a number of samples of helium atoms interacting via the Aziz poten-

tial.[19] The atoms are assumed to be in an external field $U_{sub}(z)$ describing the adhesion of the helium atoms to a graphite surface. The graphite substrate has the remarkable property that, with the exception of a few discrete densities, the experimental results can be understood completely in terms of the properties of the helium liquid alone,[20] i.e., the only role of the graphite is to confine the helium to a two-dimensional layer. A simple form for $U_{sub}(z)$ is the potential obtained by averaging Lennard-Jones interactions between helium and graphite atoms over a half-space.[21,22] One obtains

$$U_{sub}(z)=e\left[\frac{1}{15}\left[\frac{s}{z}\right]^9-\left[\frac{s}{z}\right]^3\right]. \tag{3.1}$$

The potential (3.1) is an oversimplification in the sense that the real graphite-helium potential is not translationally invariant in the x-y plane due to the crystal structure of the substrate. The breaking of translational invariance in the x-y plane is relatively weak in the special case of a graphite substrate, but it does give rise to interesting physical effects[23] at discrete densities. These effects are ignored in the present work. Moreover, the interaction between two individual helium atoms is changed in the presence of a substrate[24,25] due to the substrate screening of the van der Waals interaction. Our one-body densities near the substrate should therefore not be considered as quantitative predictions.

We have chosen here three different models of the substrate potential. Two of them use a potential of the form (3.1), and are characterized by the strength e and the range s appearing in Eq. (3.1). Model I uses a substrate potential of the form (3.1) fitted to the strength of the attractive tail[22] of the helium-graphite interaction. The potential parameters are $e=48$ K and $s=3.6$ Å, which is about midway between the theoretical and experimental predictions quoted in Ref. 22. The potential minumum is at 2.75 Å, which agrees with the value suggested in Ref. 22 for a helium atom located directly above a graphite atom. However, the attraction at the potential minimum is about a factor of 2.5 too weak. This is necessary to avoid having the HNC/EL equations for the *liquid* become unstable due to a local instability against formation of a solid.

Model II is a potential suggested by Dupont-Roc.[26] It describes a system where a thin film of solid H_2 of about 10 Å thickness is adsorbed to a glass surface. The ^{4}He atoms see the van der Waals force due to both the hydrogen and the glass substrate. The potential form is

$$U_{sub}(z)=-\frac{435}{z^3}-\frac{1.5\times10^4}{z^5}+\frac{0.9\times10^6}{z^9}-\frac{915}{(z+10)^3}. \tag{3.2}$$

[$U_{sub}(z)$ is given in K, and z in Å.] The last term is due to the attraction of the underlying glass surface. The potential is about half as strong as our model I.

Model III is an artificially weakened potential of the form (3.1) with the parameters $e=6$ K and $s=3.75$ Å. The potential is meant primarily to model the surface of a thick film of the order of 20 Å thickness. Since the computational effort involved scales as the third power of the

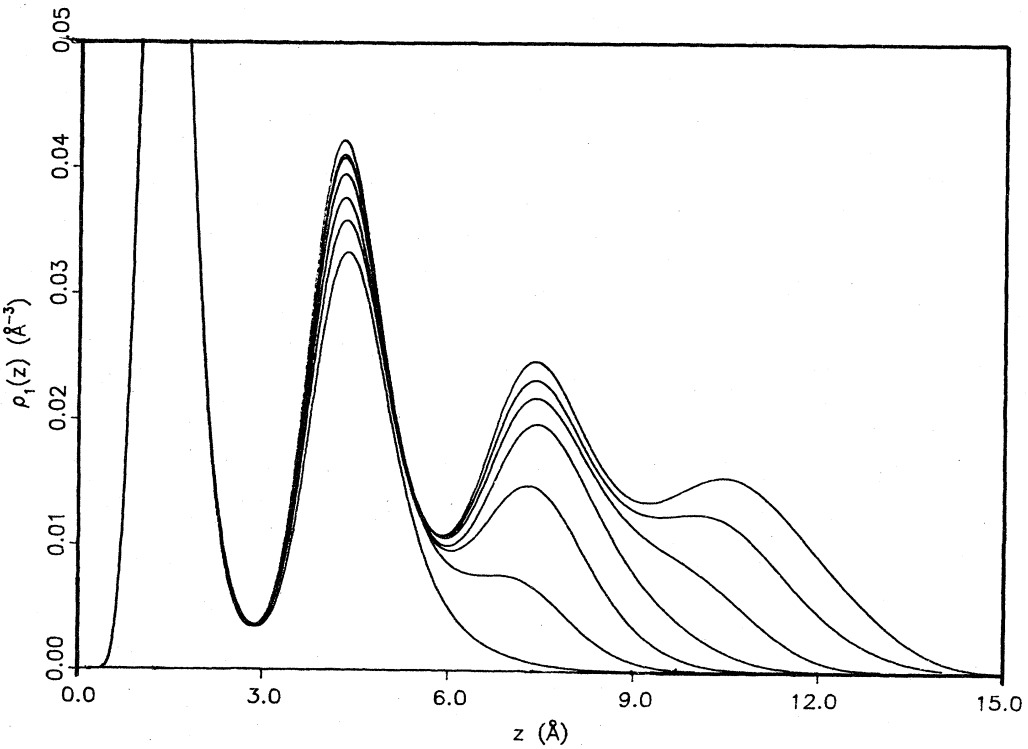

FIG. 1. Density profiles for helium films are shown, for the strong substrate potential model I, for particle numbers $n=0.14$, 0.16, 0.18, 0.20, 0.22, 0.24, and 0.26 Å^{-2}. The substrate is located at $z\leq 0$.

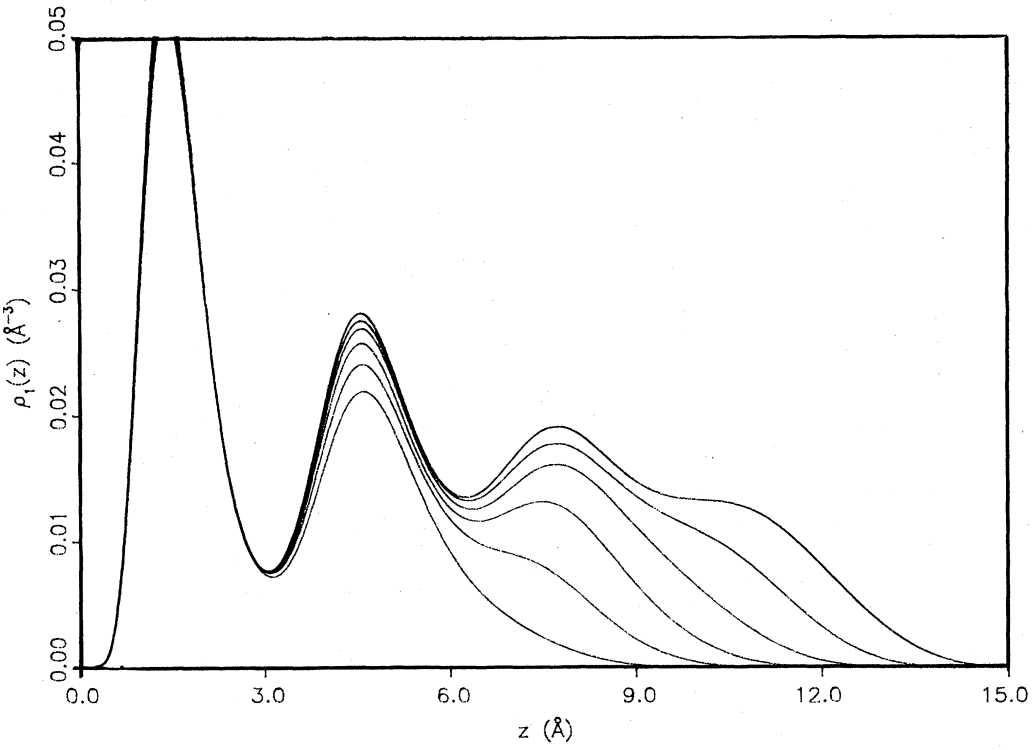

FIG. 2. Same as Fig. 1 for the substrate potential model II [Eq. (3.2)]. The surface coverages are $n=0.12$, 0.14, 0.16, 0.18, 0.20, and 0.22 Å^{-2}.

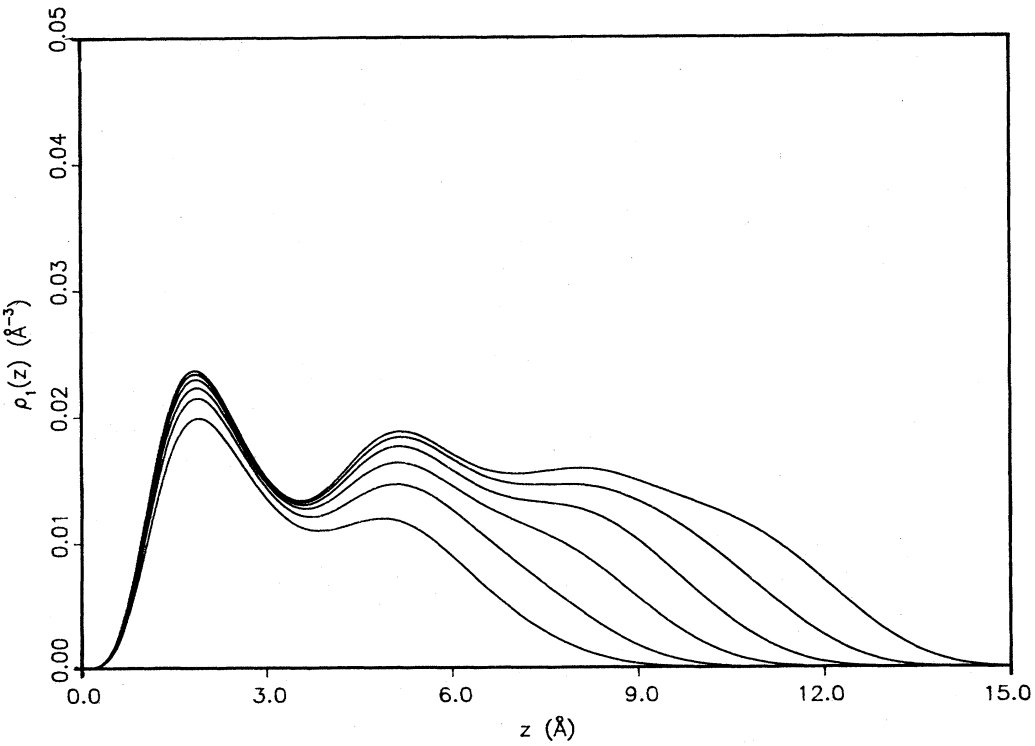

FIG. 3. Same as Fig. 1 for the weak substrate potential model III. The surface coverages are $n=0.08$, 0.10, 0.12, 0.14, 0.16, and 0.18 Å^{-2}.

film thickness, it was found more efficient to simulate the larger distance to the substrate surface by using such a potential. The repulsive part of the substrate potential must still be included in order to guarantee the boundary conditions. We believe that with these three models, we have covered a sufficiently representative sample of different physical situations.

Figures 1—3 show the one-body densities $\rho_1(z)$ for the three potential models for helium films of different surface coverages

$$n = \int \rho_1(z)dz \ . \tag{3.3}$$

The coordinate origin is chosen to be a distance $s/2$ to the right of the singularity of the substrate potential (3.1). All density profiles have a strong peak at the location where the substrate potential is most attractive. Depending on the coverage n one to three additional density maxima indicate the formation of a second, third, etc. layer of atoms. This layer structure is the main new feature appearing in our present calculations. Comparable structure has not been observed in the free films studies in I. Figure 4 shows a matching of the one-body density obtained from the model calculations I and III, shifted by about 6 Å. The first density peak of the weak-potential model agrees well with the third peak of the strong-potential model I. We also note that the two substrate potentials are very weak and roughly of the same strength in that area. The matching of those two shifted density profiles should provide a reasonably good idea of the strength of the layer structure in thicker films.

The results of model I suggest an enormous density of about five times the calculated equilibrium density at the location of the first atomic layer. We have already pointed out that the helium atoms should feel in that area the presence of the discrete structure of the substrate and a modified two-body interaction; a liquid model is certainly an inadequate description of the true physical situation. More realistic models of the two-body interaction[25] suggest that the attraction is weakened by about 20%, which should noticably decrease the peak density. The second atomic layer in that model still exhibits a peak density of about twice the saturation density of bulk ^{4}He. It is not clear to what extent this prediction is a quantitative one. It is known that the HNC approximation in *bulk* ^{4}He tends to predict too high a value for the compressibility. One could therefore conclude that an improved calculation, including elementary diagrams and three-body correlations,[27] would lead to even stronger density fluctuations. The weaker attractive part of the helium-helium potential would tend to counteract; the net effect is hard to estimate.

There is experimental evidence that the second layer, when fully populated, is also solid.[28,29] Variational calculations for bulk ^{4}He predict that the liquid phase becomes unstable against *macroscopic* admixtures of anisotropic correlations[30] at densities about 30% higher than the calculated saturation density. This is not in contradiction with the existence of *locally* stable liquid solutions of the liquid HNC/EL equations, which exist[31] up to a density of about 0.052 Å^{-3} for the present interaction. The geometric restrictions of an almost two-dimensional structure push the critical density for a local instability of the

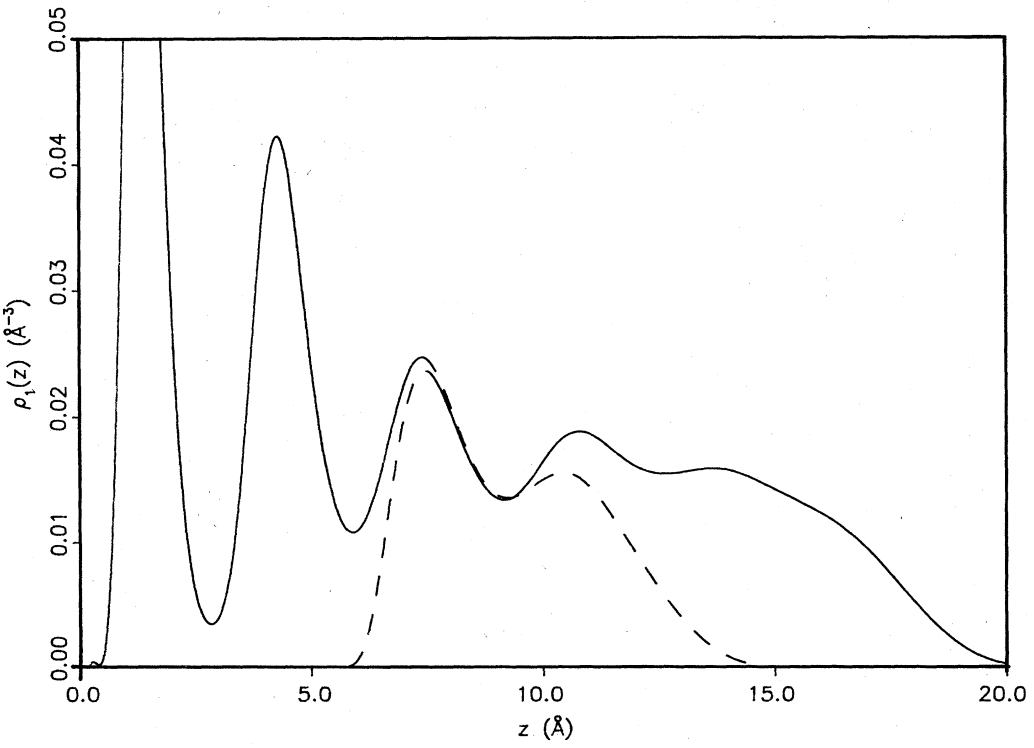

FIG. 4. Combination of the density profile of model I with $n=0.26$ Å^{-2} and a shifted model III density profile with $n=0.18$ Å^{-2}.

TABLE I. Correlation energy E_c, adhesion energy E_{sub}, total energy E energy per surface area, energy per particle E/n, and the chemical potential μ for films of a surface coverage n between 0.14 and 0.26 Å^{-2} in the strong substrate potential model I.

n (Å^{-2})	E_c (K Å^{-2})	E_{sub} (K Å^{-2})	E (K Å^{-2})	E/n (K)	μ (K)
0.14	1.03	−5.39	−4.36	−31.15	−12.02
0.16	1.01	−5.57	−4.56	−28.52	−9.66
0.18	0.90	−5.65	−4.75	−26.38	−9.08
0.20	0.84	−5.76	−4.92	−24.59	−7.78
0.22	0.79	−5.86	−5.06	−23.02	−7.07
0.24	0.72	−5.93	−5.21	−21.70	−6.72
0.26	0.63	−5.97	−5.34	−20.52	−6.23

HNC/EL equations slightly above 0.1 Å^{-3}. The qualitative features of the present model are the expected ones, but there are still too many uncertainties to make a quantitative microscopic statement about the structure of the first two layers.

Our results for the ground-state energies and the chemical potentials for the three models under consideration are collected in Tables I–III. The results of model I are interesting, because these high-density films are bound only by the external potential. The correlation energy,

$$E_c=\frac{\hbar^2}{8m}\int d^3r\rho_1(\mathbf{r})\,|\,\nabla\ln\rho_1(\mathbf{r})\,|^2+(\Delta E_2) \tag{3.4}$$

[cf. Eq. (2.4)], is positive for all surface coverages considered. Model II lies on the boundary; the films with $n<0.16$ Å^{-2} are held by the substrate potential, while those with larger particle numbers are self-bound.

The chemical potential in model I decreases rapidly with particle number. Given the uncertainties of the predictions of the structure of the first two layers, it is consistent with the experimental result of −40 K for a double layer.[32] One expects, roughly, the behavior[33]

$$\mu(d)=\mu_\infty-(\alpha_s-\alpha)/d^3\ , \tag{3.5}$$

where $\alpha_s=es^3$ is the strength of the substrate potential, α/z^3 is the van der Waals attraction of a free particle to the bulk liquid surface, and d is an approximate or "nominal" thickness of the film. For the case of a diffuse surface studied here there is no unique way to define the film thickness d. The surface width depends on the population of the last layer, and an expression of the form (3.5) can only be approximately true. One possibility is to define d as $d=n/\rho_0$, ρ_0 is some average density. Using this definition for d, $\rho_0=0.021\,85$ Å^{-3}, and the calculated asymptotic chemical potential[1] $\mu_\infty=-5.2$ K, we found in model I $(\mu-\mu_\infty)d^3\approx(\alpha_s-\alpha)$ between 1750 and 2200 K Å^3. This is in reasonable agreement with the asymptotic form of the substrate potential $es^3=2247$ K Å^3. The values for $(\mu-\mu_\infty)d^3$ vary more strongly in model II; they lie between 320 and 440 K Å^3, which must be compared with the coefficient of the $1/z^3$ term in Eq. (3.2). The last term in the expression (3.2) is still smaller. In neither of the two cases do we find that $(\mu-\mu_\infty)d^3$ is a monotonic function of d or n, which indicates the existence of corrections due to the layer structure. This is also manifested in model III, where the substrate potential is about eight times weaker, and the chemical potential is not even a monotonic function of the particle number.

As expected, the results of model III are in much closer agreement with the bulk properties of ^{4}He. Figure 5 shows the decomposition of the ground-state energy of model III into the "correlation energy" E_c [cf. Eq. (3.4)] and the "adhesion energy"

$$E_{sub}=\int dz\,\rho_1(z)U_{sub}(z)\ . \tag{3.6}$$

The correlation energy exhibits the near linear dependence on n already found in I. The extraction of a surface energy from the asymptotic expansion,

$$E(n)=\sigma_s+\sigma_f+\mu_\infty n\ , \tag{3.7}$$

is not as straightforward as in I, since there are two quite different surfaces (at the substrate boundary and at the free surface) with different surface energies σ_f and σ_s. These cannot be uniquely disentangled. Hence, an asymptotic expansion as Eq. (3.7) gives at most an average surface energy. We note that this average agrees reasonably

TABLE II. Same as Table I for films of a surface coverage n between 0.12 and 0.22 Å^{-2} in the medium-strength substrate potential model II.

n (Å^{-2})	E_c (K Å^{-2})	E_{sub} (K Å^{-2})	E (K Å^{-2})	E/n (K)	μ (K)
0.12	0.20	−1.74	−1.54	−12.80	−7.21
0.14	0.13	−1.80	−1.67	−11.92	−6.57
0.16	0.03	−1.83	−1.80	−11.28	−6.32
0.18	−0.06	−1.87	−1.93	−10.71	−5.91
0.20	−0.15	−1.89	−2.04	−10.20	−5.68
0.22	−0.25	−1.90	−2.15	−9.78	−5.51

TABLE III. Total energy E per surface area, energy per particle E/n, and the chemical potential μ for films of a surface coverage n between 0.08 and 0.16 Å^{-2} in the weak substrate potential model III. Column 5 shows the integrated condensate fraction n_c, cf. Eq. (5.24).

n (Å^{-2})	E (K Å^{-2})	E/n (K)	μ (K)	n_c
0.08	−0.35	−4.37	−5.20	0.41
0.10	−0.46	−4.57	−5.26	0.36
0.12	−0.57	−4.71	−5.31	0.34
0.14	−0.67	−4.82	−5.32	0.32
0.16	−0.78	−4.89	−5.27	0.30
0.18	−0.89	−4.95	−5.23	0.29

well with the surface tension found in I.

The "adhesion energy" (3.6) should approach an asymptotic value as d^{-2}, where d is the thickness of the film. Figure 5 shows that, even in the weak substrate potential, we have not quite reached this regime.

Our results on the static properties of the helium films are entirely consistent with those found in I. In particular, no characteristic new features of the pair-distribution function $g(\mathbf{r}_1,\mathbf{r}_2)$ have been found. The essentially new feature appearing in the present calculations is the layer structure of the one-body density. We believe that the complicated structure in the one-body density is the most convincing argument for using an *unconstrained* variational approach to the helium-substrate problem.

IV. COLLECTIVE EXCITATIONS

One of the most attractive properties of our formulation of the HNC/EL problem is that the normal modes of the system are a natural by-product of the optimization procedure. The formal basis is the formulation of linear response theory in strongly correlated inhomogeneous Bose liquids. We have described in II an excited state of the film in analogy to the Feynman phonon by writing a time-dependent wave function,

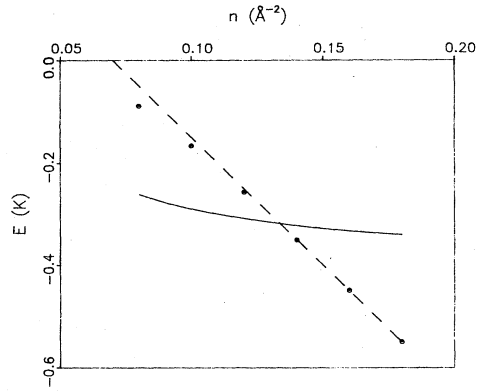

FIG. 5. "Correlation energy" E_c (small circles) and "adhesion energy" $E_{\rm sub}$ are shown, as a function of the particle number, for the (weak) potential model III. The dashed line represents a linear fit to the correlation energy.

$$|\Psi_0(t)\rangle = \exp(iH_{00}t/\hbar) \times \exp\left[\frac{1}{2}\sum_{i=1}^{A} u_1(\mathbf{r},t) + \frac{1}{2}\sum_{\substack{i,j=1\\ i<j}}^{A} u_2(\mathbf{r}_i,\mathbf{r}_j)\right]\Big/\mathcal{N}\,, \tag{4.1}$$

where $\mathcal{N}$ is the norm. We assume further that the amplitude of the time-dependent portion of the one-body correlations is small such that one may linearize the equations of motion for $\delta u_1(\mathbf{r},t)\equiv u_1(\mathbf{r},t)-u_1(\mathbf{r})$. These equations are derived from an action integral,

$$\mathcal{L} = \int dt \langle \Psi_0(t)\,|\, H + U_{\rm ext}(\mathbf{r},t) - i\hbar\frac{\partial}{\partial t}\,|\,\Psi_0(t)\rangle\,, \tag{4.2}$$

by requiring stationarity with respect to the time-dependent component of the wave function,

$$\delta\mathcal{L} = 0\,. \tag{4.3}$$

$U_{\rm ext}(\mathbf{r},t)$ is a small, time-dependent external field. We note that meaningful equations of motion can be formulated only on top of an optimized ground state. If the ground state does not minimize the energy within the space of trial functions, one must always expect spurious instabilities which indicate that a better wave function can be found.

Fourier decomposing the perturbing field,

$$U_{\rm ext}(\mathbf{r},t) = U_{\rm ext}(\mathbf{r})(e^{i\omega t}+e^{-i\omega t})\,, \tag{4.4}$$

and the time-dependent induced density fluctuation, we derived in II an expression for the density-density response function

$$\chi^{-1}(\mathbf{r}_1,\mathbf{r}_2;\omega) = \chi_0^{-1}(\mathbf{r}_1,\mathbf{r}_2;\omega) - V_{\text{p-h}}(\mathbf{r}_1,\mathbf{r}_2)\,, \tag{4.5}$$

where $V_{\text{p-h}}(\mathbf{r}_1,\mathbf{r}_2)$ is the particle-hole interaction (2.11b), (2.11c), and $\chi_0(\mathbf{r}_1,\mathbf{r}_2)$ is the density-density response function of the "noninteracting" system characterized by the one-body Hamiltonian (2.12). In the spectral decomposition,

$$H_1(\mathbf{r}_1,\mathbf{r}_2) = \sum_i e_i\phi_i(\mathbf{r}_1)\phi_i(\mathbf{r}_2)\,, \tag{4.6}$$

$\chi_0(\mathbf{r}_1,\mathbf{r}_2;\omega)$ has the canonical form

$$\chi_0(\mathbf{r}_1,\mathbf{r}_2;\omega) = 2\sum_i \frac{\rho_1^{1/2}(\mathbf{r}_1)\phi_i(\mathbf{r}_1)e_i\phi_i(\mathbf{r}_2)\rho_1^{1/2}(\mathbf{r}_2)}{\hbar^2\omega^2-e_i^2}\,. \tag{4.7}$$

The normal modes of the system are the nontrivial solutions of the equation

$$\int d^3r_2\,\chi(\mathbf{r}_1,\mathbf{r}_2;\omega)\delta\rho_1(\mathbf{r}_2;\omega) = 0\,. \tag{4.8}$$

We have shown in I and II that the most economical way to solve the RPA equation (2.11a) is to consider the eigenvalue problem

$$\int d^3r_2\{\delta(\mathbf{r}_1-\mathbf{r}_2)H_1(\mathbf{r}_2) + 2[\rho_1(\mathbf{r}_1)]^{1/2}V_{\text{p-h}}(\mathbf{r}_1,\mathbf{r}_s)[\rho_1(\mathbf{r}_2)]^{1/2}\} \times H_1(\mathbf{r}_2)\psi_l(\mathbf{r}_2) = \hbar^2\omega_l^2\psi_l(\mathbf{r}_1)\,. \tag{4.9}$$

From the solutions of Eq. (4.9) we can construct the pair distribution function

$$g(\mathbf{r}_1,\mathbf{r}_2)=1+\frac{1}{[\rho_1(\mathbf{r}_1)]^{1/2}} \times\left[\sum_l \frac{1}{\hbar\omega_l}[H_1(\mathbf{r}_1)\psi_l(\mathbf{r}_1)][H_1(\mathbf{r}_2)\psi_l(\mathbf{r}_2)] -\delta(\mathbf{r}_1-\mathbf{r}_2)\right]\frac{1}{[\rho_1(\mathbf{r}_2)]^{1/2}}, \quad (4.10)$$

and the non-nodal diagrams $X(\mathbf{r}_1,\mathbf{r}_2)$. During that proof, it was also shown that the density fluctuations of the system are given by

$$\delta\rho_1^{1/2}(\mathbf{r};\omega)=\frac{\delta\rho_1(\mathbf{r};\omega)}{2[\rho_1(\mathbf{r})]^{1/2}}=[H_1(\mathbf{r})\psi_l(\mathbf{r})]\delta(\omega-\omega_l)\,. \quad (4.11)$$

Our approach to the excited states is similar to that of Chang and Cohen,[34] and one can derive their formulation by eliminating the particle-hole interaction in favor of the pair-distribution function, using the Euler-Lagrange equation (2.11a). The important new feature of our optimized treatment of the ground state is that the static form factor, and hence the pair distribution function, is consistent with the elementary excitations in the sense of the fluctuation-dissipation theorem.

Figures 6 and 7 show the dispersion relations for the five lowest-lying elementary excitations of helium films in the weak and strong substrate potentials, respectively, as a function of the momentum q parallel to the surface. There are no continuum states due to the confinement of the film in the z direction. A feature common to both sets of dispersion relations is the closeness of the two lowest-lying modes at $q\approx 1.5$ Å^{-1}, which suggests a level-crossing effect in that momentum region. A similar effect has been observed in II, where we could attribute the feature to a level crossing between the surface (ripplon) and the volume (zero sound) excitations. A similar level crossing has been predicted by Chang and Cohen[34] and by Woo.[35] The situation is more complicated in the present case since we can have two qualitatively different surface excitations: one at the free surface, and the other at the substrate boundary.

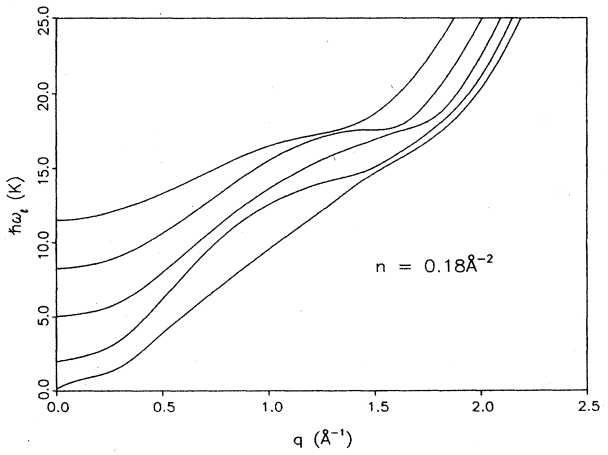

FIG. 6. Dispersion relations of the five lowest-lying modes are shown for the film with $n=0.18$ Å^{-2} in the weak substrate potential III.

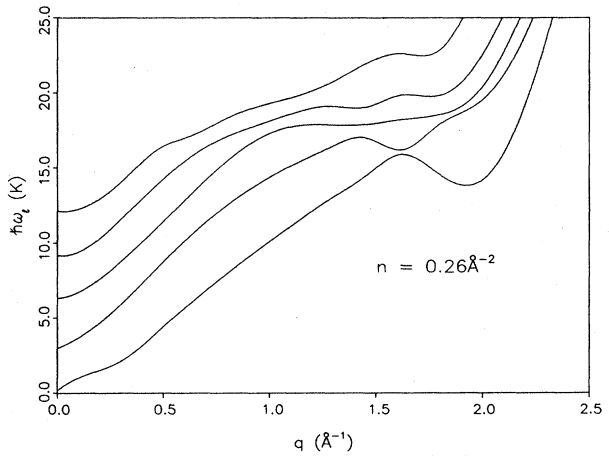

FIG. 7. Same as Fig. 6 for the film with $n=0.26$ Å^{-2} in the strong substrate potential I.

The physical situation is clarified by considering the wave shapes of the two lowest collective modes, see Figs. 8 and 9. Up to a momentum of about 1.5 Å^{-1}, the lowest-lying mode in the *weak* potential (see Fig. 8) is an excitation of the free surface; the next one is an excitation close to the substrate boundary. Both modes, of course, have a considerable overlap for wavelengths longer than the film thickness. In particular at $q=0$, the second excited state looks like a superposition of excitations of both surfaces, much like the antisymmetric modes of the free films studied in II. The identification as excitations at the free surface and the substrate boundary becomes clearer with increasing wave number.

Between a momentum of 1.5 and 1.6 Å^{-1}, there is obviously a level crossing between the two surface modes, and the one at the substrate boundary becomes energetically lower. This effect has not been observed in the case of free films studied in I and II. However, at slightly larger wave numbers, we find a second change of the wave shape into one bulk mode and one excitation at the substrate boundary. Both level crossings are probably caused by the approaching zero-sound mode, which is the lowest-lying excitation at $q>2$ Å^{-1}. It is unfortunately impossible to identify the bulk mode with one of the higher-lying states at long wavelengths. These states have two or more nodes, and are extended over the full thickness of the film. It cannot be clearly decided whether a given mode is a bulk excitation or a superposition of two surface modes.

The character of the different elementary excitations is most clearly identified for the case of the thickest film in the weak substrate potential. At the smaller surface coverages, the overlap between the excitations of both surfaces increases, which makes an identification of the different excitations less obvious.

The waveforms of the excitations in the strong substrate potential are qualitatively somewhat different. Figure 9 shows that over a wide regime of wave numbers,

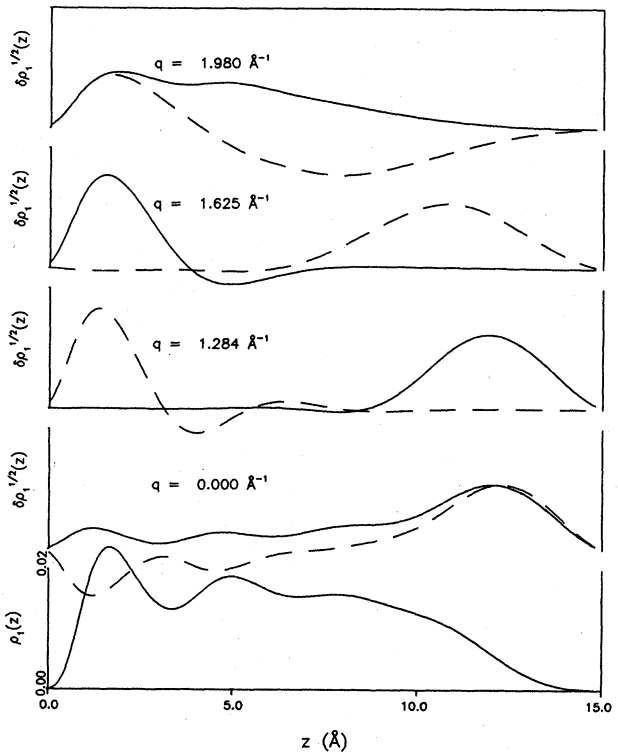

FIG. 8. Waveforms of two lowest-lying collective excitations are shown for, the weak substrate potential model III, and four different wave numbers q parallel to the surface (upper four curves). The solid lines represent the waveform of the lowest-lying state, the dashed line the one of the second excitation. Also shown is, for comparison, the one-body density of the underlying model calculation with $n=0.18$ Å^{-2} (bottom curve). Note the change of the waveform between $q=1.45$, 1.625, and 1.98 Å^{-2}.

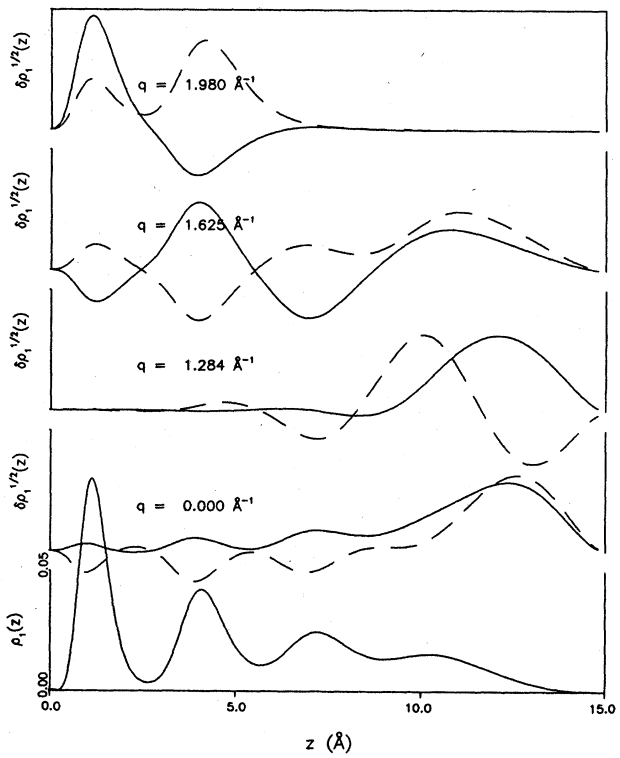

FIG. 9. Same as Fig. 8 for the strong substrate potential.

both of the two lowest-lying modes are free surface excitations. It is tempting to identify one of them as a ripplon mode (i.e., a surface-tension driven excitation), the other one as third sound (i.e., a substrate-potential driven excitation).[36] It is then also plausible that the second surface mode does not appear in the films in the weak substrate potential. From the present calculation it can not be decided which of two given modes should be called the "ripplon," and which one "third sound." Again, the level crossing around $q=1.5$ Å^{-1} is caused by a migration of the lowest-lying mode from the free surface to the substrate boundary. This migration is slower than in the case of the weak substrate potential, and is accompanied by the migration of the *second* mode to an excitation of the second atomic layer. A clear bulk mode could not be identified; the higher-lying modes are strongly modulated by the strong variation of the equilibrium density.

V. DENSITY MATRIX

Given the wave function (1.1) and assuming that the correlations are known, we may now proceed to calculate the full one-body density matrix

$$\rho_1(\mathbf{r},\mathbf{r}')=A\frac{\int d^3r_2\int d^3r_3\cdots\int d^3r_A\,\Psi_0(\mathbf{r},\mathbf{r}_2,\mathbf{r}_3,\ldots,\mathbf{r}_A)\Psi_0(\mathbf{r}',\mathbf{r}_2,\mathbf{r}_3,\ldots,\mathbf{r}_A)}{\int d^3r_1\int d^3r_2\cdots\int d^3r_A\,|\Psi_0(\mathbf{r}_1,\mathbf{r}_2,\ldots,\mathbf{r}_A)|^2}\,. \tag{5.1}$$

We do not introduce a special notation to distinguish the one-body density matrix $\rho_1(\mathbf{r},\mathbf{r}')$ from its diagonal limit

$$\rho_1(\mathbf{r})\equiv\rho_1(\mathbf{r},\mathbf{r})\,; \tag{5.2}$$

the notation will be made unambiguous by explicit display of the non-trivial coordinate dependence. The density matrix is needed for the finite-temperature extension of the theory[14,15] and the interpretation of neutron scattering experiments. An especially interesting quantity is the limit of large distances $|\mathbf{r}_1-\mathbf{r}_2|$,

$$\rho_1(\mathbf{r}_1,\mathbf{r}_2)\rightarrow[\rho_1(\mathbf{r}_1)n_c(\mathbf{r}_1)\rho_1(\mathbf{r}_2)n_c(\mathbf{r}_2)]^{1/2}$$

$$(|\mathbf{r}_1-\mathbf{r}_2|\rightarrow\infty)\,. \tag{5.3}$$

This limit gives information on the coherent structure of

the ground state.[37] Related to this is the question of superfluidity, which has been detected in films as thin as two atomic layers.[38] (We note that the present theory, which assumes *zero temperature*, is not immediately comparable to the Kosterlitz-Thouless theory of vortex binding which applies to *finite temperature*.) $n_c(\mathbf{r})$ is, in the bulk limit, the fraction of particles occupying the zero-momentum Bose-Einstein condensate. The momentum is no longer a good quantum number in an inhomogeneous system. For the films under consideration here, we may identify $n_c(\mathbf{r})$ with the fraction of particles at location z having zero momentum parallel to the surface.

The variational theory for the density matrix in an inhomogeneous system has not yet been worked out in the literature; we must therefore review the basic steps of the derivation. Our analysis follows largely a suggestion by Feenberg[39] which does not rely on cluster expansions in terms of the pair correlations $h_2(\mathbf{r}_1,\mathbf{r}_2)=\exp[u_2(\mathbf{r}_1,\mathbf{r}_2)]-1$ as an intermediate step.

Let

$$h_2(\mathbf{r},\mathbf{r}';\mathbf{r}_1)=\exp\{[u_2(\mathbf{r},\mathbf{r}_1)+u_2(\mathbf{r}',\mathbf{r}_1)]/2\}-1\ , \tag{5.4}$$

and

$$I_A=\int d^3r_1\int d^3r_2\cdots\int d^3r_A\,|\,\Psi_0(\mathbf{r}_1,\mathbf{r}_2,\ldots,\mathbf{r}_A)\,|^2\ . \tag{5.5}$$

Using the definitions of the n-particle distribution functions of an A-particle system,

$$\rho(\mathbf{r}_1,\mathbf{r}_2,\ldots,\mathbf{r}_n)=\frac{A!}{(A-n)!I_A}\int d^3r_{n+1}\int d^3r_{n+2}\cdots\int d^3r_A\,|\,\Psi_0(\mathbf{r}_1,\mathbf{r}_2,\ldots,\mathbf{r}_A)\,|^2\ , \tag{5.6}$$

we find

$$\rho_1(\mathbf{r},\mathbf{r}')=A\frac{I_{A-1}}{I_A}\exp\{[u_1(\mathbf{r})+u_1(\mathbf{r}')]/2\}\times\left[1+\int d^3r_1\,h_2(\mathbf{r},\mathbf{r}',\mathbf{r}_1)\rho_1(\mathbf{r}_1)+\frac{1}{2!}\int d^3r_1\int d^3r_2\,h_2(\mathbf{r},\mathbf{r}';\mathbf{r}_1)h_2(\mathbf{r},\mathbf{r}';\mathbf{r}_1)\rho_2(\mathbf{r}_1,\mathbf{r}_2)+\cdots\right]. \tag{5.7}$$

Next, decompose the n-particle densities into the cluster functions[40]

$$\begin{aligned}
&p_1(\mathbf{r}_1)=\rho_1(\mathbf{r}_1)\ ,\\
&p_2(\mathbf{r}_1,\mathbf{r}_2)=\rho_2(\mathbf{r}_1,\mathbf{r}_2)-\rho_1(\mathbf{r}_1)\rho_1(\mathbf{r}_2)\ ,\\
&p_3(\mathbf{r}_1,\mathbf{r}_2,\mathbf{r}_3)=\rho_3(\mathbf{r}_1,\mathbf{r}_2,\mathbf{r}_3)-\rho_1(\mathbf{r}_1)\rho_2(\mathbf{r}_1,\mathbf{r}_2)-\rho_1(\mathbf{r}_2)\rho_2(\mathbf{r}_1,\mathbf{r}_3)-\rho_1(\mathbf{r}_3)\rho_2(\mathbf{r}_1,\mathbf{r}_2)+2\rho_1(\mathbf{r}_1)\rho_1(\mathbf{r}_2)\rho_1(\mathbf{r}_3)\ .\\
&\quad\cdots
\end{aligned} \tag{5.8}$$

Note that the cluster functions $p_n(\mathbf{r}_1,\ldots,\mathbf{r}_n)$ satisfy the "cluster property," i.e., they vanish whenever one or more of the particles is moved far away from the others. Inserting the cluster functions (5.8) and their higher-order generalizations into (5.7), one finds

$$\rho_1(\mathbf{r},\mathbf{r}')=A\frac{I_{A-1}}{I_A}\exp\left[[u_1(\mathbf{r})+u_1(\mathbf{r}')]/2+\int d^3r_1 h_2(\mathbf{r},\mathbf{r}';\mathbf{r}_1)p_1(\mathbf{r}_1)+\tfrac{1}{2}\int d^3r_1 d^3r_2 h_2(\mathbf{r},\mathbf{r}',\mathbf{r}_1)h_2(\mathbf{r},\mathbf{r}',\mathbf{r}_2)p_2(\mathbf{r}_1,\mathbf{r}_2)+\cdots\right]\equiv A\frac{I_{A-1}}{I_A}\exp[q(\mathbf{r},\mathbf{r}')]\ . \tag{5.9}$$

The ratio I_A/I_{A-1} can be derived from Eq. (5.9), by letting $\mathbf{r}=\mathbf{r}'$ in $h_2(\mathbf{r},\mathbf{r}';\mathbf{r}_i)$. We find

$$\frac{I_A}{I_{A-1}}=\int\exp[q(\mathbf{r},\mathbf{r})]d^3r\ , \tag{5.10}$$

and hence

$$\rho_1(\mathbf{r},\mathbf{r}')=A\frac{\exp[q(\mathbf{r},\mathbf{r}')]}{\int\exp[q(\mathbf{r},\mathbf{r})]d^3r}\ . \tag{5.11}$$

We finally eliminate the normalization integral by taking the diagonal limit $\mathbf{r}=\mathbf{r}'$ in Eq. (5.11):

$$\rho_1(\mathbf{r})=A\frac{\exp[q(\mathbf{r},\mathbf{r})]}{\int\exp[q(\mathbf{r},\mathbf{r})]d^3r} \tag{5.12}$$

and find

$$\rho_1(\mathbf{r},\mathbf{r}')=[\rho_1(\mathbf{r})\rho_1(\mathbf{r}')]^{1/2}\exp[q(\mathbf{r},\mathbf{r}')-\tfrac{1}{2}q(\mathbf{r},\mathbf{r})-\tfrac{1}{2}q(\mathbf{r}',\mathbf{r}')]\ . \tag{5.13}$$

Note that the identity $\rho_1^{-1}(\mathbf{r})\exp[q(\mathbf{r},\mathbf{r})]=\text{const}$ is not necessarily fulfilled in an approximate expression for the one-body density and the function $q(\mathbf{r},\mathbf{r})$. Rather, the identity forms a consistency test on the approximations in use.

The off-diagonal limit $|\mathbf{r}-\mathbf{r}'|\to\infty$ is obtained by expanding

$$h_2(\mathbf{r},\mathbf{r}';\mathbf{r}_1)=\{\exp[u_2(\mathbf{r},\mathbf{r}_1)]-1\}\{\exp[u_2(\mathbf{r}',\mathbf{r}_1)]-1\}+\{\exp[u_2(\mathbf{r},\mathbf{r}_1)]-1\}+\{\exp[u_2(\mathbf{r}',\mathbf{r}_1)]-1\}\ . \tag{5.14}$$

Subtracting the off-diagonal limit of $q(\mathbf{r},\mathbf{r}')$,

$$q(\mathbf{r},\mathbf{r}')\equiv D_f(\mathbf{r})+D_f(\mathbf{r}')-Q(\mathbf{r},\mathbf{r}') ,$$
$$Q(\mathbf{r},\mathbf{r}')\to 0 \quad (|\mathbf{r}-\mathbf{r}'|\to\infty) , \tag{5.15}$$

we arrive at our final representation of the density matrix,

$$\rho_1(\mathbf{r},\mathbf{r}')=[\rho_1(\mathbf{r})\rho_1(\mathbf{r}')n_c(\mathbf{r})n_c(\mathbf{r}')]^{1/2}\exp[Q(\mathbf{r},\mathbf{r}')] , \tag{5.16}$$

where

$$n_c(\mathbf{r})=\exp[2D_f(\mathbf{r})-D_h(\mathbf{r})] , \tag{5.17a}$$

$$D_h(\mathbf{r})\equiv q(\mathbf{r},\mathbf{r}) . \tag{5.17b}$$

Equations (5.16) and (5.17) are the proper generalizations of the working formulas of Ref. 17 to the inhomogeneous case. In order to facilitate the identification we have used a notation as close as possible to the one of Ref. 17. The representation is exact; the relevant ingredients may now be calculated either by using the cluster expansion (5.9) to some finite order,[41] or by summing infinite classes of diagrams by an integral equation method.[18] The cluster expansions for $D_f(\mathbf{r})$ and $D_h(\mathbf{r})$ are topologically identical, differing only in that all functions $\exp[u_2(\mathbf{r},\mathbf{r}_i)/2]-1$ occurring in $D_f(\mathbf{r})$ are replaced by functions $\exp[u_2(\mathbf{r},\mathbf{r}_i)]-1$ in $D_h(\mathbf{r})$. Here, $\mathbf{r}$ is the coordinate of the *external* point.

The first few cluster contributions to $D_f(\mathbf{r})$, $D_h(\mathbf{r})$, and $Q(\mathbf{r},\mathbf{r}')$ are shown in Fig. 10. The usual[17] graphical conventions are used: The wavy line represents a factor, $\exp[u_2(\mathbf{r},\mathbf{r}_i)/2]-1$, the dashed line a factor, $\exp[u_2(\mathbf{r},\mathbf{r}_i)]-1$, and the solid line a distribution function, $g(\mathbf{r},\mathbf{r}')-1$. Solid dots indicate a density factor $\rho_1(\mathbf{r}_i)$, and imply integration over the associated coordinate space. The leading terms in $D_f(\mathbf{r})$, $D_h(\mathbf{r})$, and $Q(\mathbf{r},\mathbf{r}')$ containing the one-body factor $u_1(\mathbf{r})$ are not spelled out explicitly.

Occasionally, the success and simplicity of the HNC integral equation technique for energy calculations has led to a certain enthusiasm and blind faith in the method. Later studies have pinpointed the reason for the success of the HNC method for energy calculations: the method provides an approximate, self-consistent summation of ring and ladder diagrams; in particular it is exact in the short- and the long-range limits[42]). In I, we have proven that this statement also holds in the inhomogeneous case.

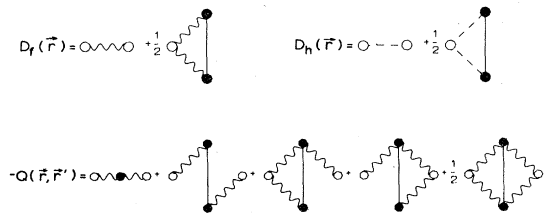

FIG. 10. The first few diagrammatic contributions to $D_f(\mathbf{r})$, $D_h(\mathbf{r})$, and $Q(\mathbf{r},\mathbf{r}')$. The diagrammatic conventions are explained in the text. The shown combination of diagrams satisfies the identity (5.21). All but the last diagram are included in the HNC summations.

The HNC technique has also been tried for other quantities, including the density matrix.[18] But we will see (see also Refs. 43 and 44 for recent numerical studies) that the HNC method for the density matrix leads to the *incorrect* answer in the limit of short distances $|\mathbf{r}-\mathbf{r}'|$, whereas the long-ranged correlations are correctly described by the second-order term of the compact cluster expansion for $Q(\mathbf{r},\mathbf{r}')$, more specifically, by the contributions of the first and second diagram of Fig. 10 to $Q(\mathbf{r},\mathbf{r}')$. On the other hand we will see that the HNC approximation for the one-body quantities $D_f(\mathbf{r})$ and $D_h(\mathbf{r})$ is not plagued by such inconsistencies.

The derivation of HNC equations for the density matrix is a somewhat formal exercise, especially for Bose systems. As in the HNC theory for the distribution function one introduces sets of "nodal" and "non-nodal" diagrams, the only additional diagrammatic structures being objects which have a factor $\exp[u_2(\mathbf{r},\mathbf{r}_i)/2]-1$ attached to a specific external point $\mathbf{r}$. These objects carry a subscript f; note that they are not symmetric functions of the two coordinates. (We adopt the convention that in a two-body quantity the function $\exp[u_2(\mathbf{r},\mathbf{r}_i)/2]-1$ is attached to the first coordinate appearing in the argument.) The HNC equations are (we omit "elementary diagrams")

$$X_f(\mathbf{r}_1,\mathbf{r}_2)=\exp[u_2(\mathbf{r}_1,\mathbf{r}_2)/2+N_f(\mathbf{r}_1,\mathbf{r}_2)]-1-N_f(\mathbf{r}_1,\mathbf{r}_2) , \tag{5.18a}$$

$$N_f(\mathbf{r}_1,\mathbf{r}_2)=\int d^3r_3\, X_f(\mathbf{r}_1,\mathbf{r}_3)[g(\mathbf{r}_3,\mathbf{r}_2)-1] . \tag{5.18b}$$

Given $X_f(\mathbf{r}_1,\mathbf{r}_2)$, $N_f(\mathbf{r}_1,\mathbf{r}_2)$, and the ordinary graphical quantities of HNC theory $X(\mathbf{r}_1,\mathbf{r}_2)$, $N(\mathbf{r}_1,\mathbf{r}_2)$, and $g(\mathbf{r}_1,\mathbf{r}_2)$ [cf. Eqs. (2.7)], one has, in the HNC approximation,

$$D_f(\mathbf{r})=\tfrac{1}{2}u_1(\mathbf{r})+\int d^3r'\,\rho_1(\mathbf{r}')X_f(\mathbf{r},\mathbf{r}') +\tfrac{1}{2}\int d^3r'\,N_f(\mathbf{r},\mathbf{r}')\rho_1(\mathbf{r}')[X_f(\mathbf{r},\mathbf{r}')+N_f(\mathbf{r},\mathbf{r}')] , \tag{5.19a}$$

$$D_h(\mathbf{r})=u_1(\mathbf{r})+\int d^3r'\,\rho_1(\mathbf{r}')X(\mathbf{r},\mathbf{r}') +\tfrac{1}{2}\int d^3r'\,N(\mathbf{r},\mathbf{r}')\rho_1(\mathbf{r}')[X(\mathbf{r},\mathbf{r}')+N(\mathbf{r},\mathbf{r}')] , \tag{5.19b}$$

and

$$-Q(\mathbf{r},\mathbf{r}')=\int d^3r_1\, X_f(\mathbf{r},\mathbf{r}_1)\rho_1(\mathbf{r}_1)X_f(\mathbf{r}',\mathbf{r}_1) +\int d^3r_1\int d^3r_2\, X_f(\mathbf{r},\mathbf{r}_1)\rho_1(\mathbf{r}_1) \times[g(\mathbf{r}_1,\mathbf{r}_2)-1]\rho_1(\mathbf{r}_2)X_f(\mathbf{r}',\mathbf{r}_2) . \tag{5.20}$$

We will shortly see that the approximation for $Q(\mathbf{r},\mathbf{r}')$ generated by Eqs. (5.18)—(5.20) is suspect. An approximation for the density matrix within an accuracy comparable to that of the HNC method for the energy would require that the HNC approximation for $Q(\mathbf{r},\mathbf{r}')$ be exact for $|\mathbf{r}-\mathbf{r}'|\to 0$ and $|\mathbf{r}-\mathbf{r}'|\to\infty$. The *long-ranged* limit is correctly reproduced by both the compact cluster expansion of Ref. 17, and by the HNC approximation. The limit $|\mathbf{r}-\mathbf{r}'|\to 0$ is also known; from $\rho_1(\mathbf{r},\mathbf{r})=\rho_1(\mathbf{r})$, we conclude

$$2D_f(\mathbf{r})-Q(\mathbf{r},\mathbf{r})-D_h(\mathbf{r})=0\ . \tag{5.21}$$

From the diagrams shown in Fig. 10, it is easily seen how the identity (5.21) holds in any order of a properly classified cluster expansion. Unfortunately, the HNC method identifies the last diagram and corresponding higher-order ones (see Fig. 11) as elementary and suggests that these terms must be put in by hand at each order. In other words, the last diagram shown in Fig. 10 (and all the diagrams of the structure shown second in Fig. 11) is omitted for $\mathbf{r}\neq\mathbf{r}'$, but kept [embedded in $2D_f(\mathbf{r})-D_h(\mathbf{r})$] for $\mathbf{r}=\mathbf{r}'$. This inconsistency violates Eq. (5.21) in the HNC approximation. In fact, in the HNC approximation *none* of the nonelementary diagrams for $Q(\mathbf{r},\mathbf{r}')$ are treated on the same footing as those included in the HNC approximation for $2D_f(\mathbf{r})-D_h(\mathbf{r})$.

The violation of Eq. (5.21) is usually regarded as a measure of the importance of elementary diagrams. Our analysis shows that this is incorrect: The inconsistency of the diagonal limit of the HNC approximation for the density matrix is a measure of the nonelementary diagrams that are kept in $2D_f(\mathbf{r})-D_h(\mathbf{r})$, but ignored in $Q(\mathbf{r},\mathbf{r})$.

A simple remedy would be to *define* the combination $2D_f(\mathbf{r})-D_h(\mathbf{r})$ to be consistent with $Q(\mathbf{r},\mathbf{r}')$ through the identity (5.21); in other words one might omit all diagrams for $\mathbf{r}=\mathbf{r}'$ that are also omitted for $\mathbf{r}\neq\mathbf{r}'$. This is probably adequate in nuclear systems, where the omitted nonelementary diagrams are small, but dangerous in the helium liquids. An interesting alternative is a scaling procedure suggested by Puoskari and Kallio,[44] but it is not clear how to generalize such a procedure to the inhomogeneous case. We regard the HNC method, in general, as a unreliable scheme for calculating $Q(\mathbf{r},\mathbf{r}')$.

The situation is somewhat different if we restrict ourselves to the "condensate fraction," which needs only the function $2D_f(\mathbf{r})-D_h(\mathbf{r})$. Since the inadequacy of the HNC equations may be solely attributed to inadequacies in the representation of $Q(\mathbf{r},\mathbf{r}')$ for $\mathbf{r}\approx\mathbf{r}'$; we may use the HNC equations as long as we restrict our attention to the long-ranged, off-diagonal limit of the density matrix.

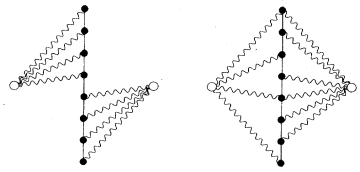

FIG. 11. Two typical diagrams contributing to $Q(\mathbf{r},\mathbf{r}')$ of a class that must be kept together to satisfy the identity (5.21). The first one is included in the HNC summation, the second one is classified as "elementary" and omitted.

It is straightforward to verify that the HNC approximation (5.19b) for $D_h(\mathbf{r})$ satisfies the identity (5.12) [cf. Eq. (5.17b)]. The proof is carried out by differentiating Eq. (5.19b) and using the HNC equations to obtain

$$\nabla D_h(\mathbf{r})=\nabla\ln\rho_1(\mathbf{r})\ . \tag{5.22}$$

Since only the combination $2D_f(\mathbf{r})-D_h(\mathbf{r})$ is needed for calculating the condensate fraction, it is convenient to rewrite the equations in terms of $\Delta X(\mathbf{r},\mathbf{r}')\equiv X_f(\mathbf{r},\mathbf{r}')-\frac{1}{2}X(\mathbf{r},\mathbf{r}')$. This has the advantage that the substantial cancellations between $2D_f(\mathbf{r})$ and $D_h(\mathbf{r})$ are automatically taken into account, thus improving the convergence of numerical calculations. Also, the correlation factors $u_1(\mathbf{r})$ and $u_2(\mathbf{r}_1,\mathbf{r}_2)$ are eliminated in favor of the physical distribution functions, and no long-ranged quantities appear.

The final form of our equations after this reformulation is

$$\Delta X(\mathbf{r}_1,\mathbf{r}_2)=[g(\mathbf{r}_1,\mathbf{r}_2)]^{1/2}\exp[\Delta N(\mathbf{r}_1,\mathbf{r}_2)]-\tfrac{1}{2}g(\mathbf{r}_1,\mathbf{r}_2)-\tfrac{1}{2}-\Delta N(\mathbf{r}_1,\mathbf{r}_2)\ , \tag{5.23a}$$

$$\Delta N(\mathbf{r}_1,\mathbf{r}_2)=\int d^3r_3\,\rho_1(\mathbf{r}_3)\Delta X(\mathbf{r}_1,\mathbf{r}_3)[g(\mathbf{r}_3,\mathbf{r}_2)-1]\ , \tag{5.23b}$$

$$\begin{aligned}D_f(\mathbf{r}_1)-\tfrac{1}{2}D_h(\mathbf{r}_1)=&\int d^3r_2\,\rho_1(\mathbf{r}_2)\Delta X(\mathbf{r}_1,\mathbf{r}_2)-\tfrac{1}{2}\int d^3r_2\,[\Delta X(\mathbf{r}_1,\mathbf{r}_2)+\Delta N(\mathbf{r}_1,\mathbf{r}_2)]\rho_1(\mathbf{r}_2)\Delta N(\mathbf{r}_1,\mathbf{r}_2)\\&-\tfrac{1}{2}\int d^3r_2\,\Delta N(\mathbf{r}_1,\mathbf{r}_2)\rho_1(\mathbf{r}_2)[g(\mathbf{r}_1,\mathbf{r}_2)-1]+\tfrac{1}{8}\int d^3r_2[g(\mathbf{r}_1,\mathbf{r}_2)-1]\rho_1(\mathbf{r}_2)N(\mathbf{r}_1,\mathbf{r}_2)\ .\end{aligned} \tag{5.23c}$$

Equations (5.23) have been solved on the background of the helium-film calculations of model III discussed in Sec. III. This model has been chosen since it gives a better representation of the behavior of the local condensate fraction in the vicinity of the surface of bulk ^{4}He. The local condensate fractions (i.e., the fraction of particles in the zero momentum state parallel to the surface, at a certain distance z from the substrate) are shown in Fig. 12; the integrated condensate fractions,

$$n_c=\frac{\int\rho_1(z)n_c(z)dz}{\int\rho_1(z)dz}\ , \tag{5.24}$$

are given in Table III. We find, as expected, that the condensate fraction increases with decreasing density; the locations of the minima of the condensate fraction shown in Fig. 12 agree essentially with the locations of the density

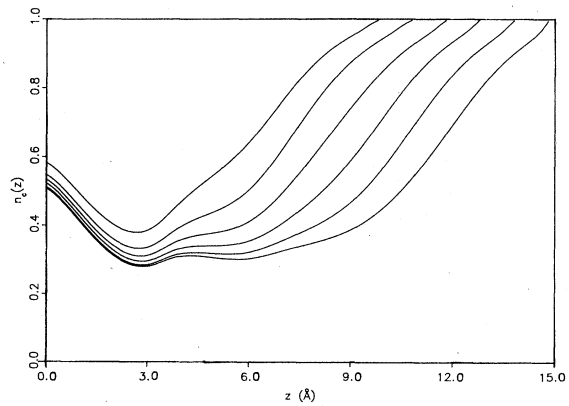

FIG. 12. Local condensate fractions $n_c(z)$ are shown for the helium films in the weak substrate potential.

maxima shown in Fig. 3. The trend persists in models I and II; the condensate fraction within the first (model II) and the first two (model I) layers is virtually zero. Thus, the largest portion of the condensed phase resides in the low-density outer layers of the film. This fact lends reliability to the model in the sense that it does not predict a significant condensate fraction in areas where one should expect that the liquid model is unphysical. As a result of the HNC approximation, the density profiles obtained in Sec. III are somewhat lower than what one would expect from experiments. Improvements of our calculations should therefore lead to slightly smaller condensate fractions, especially in the high-density regimes, without changing the overall picture very much.

VI. IMPURITY POTENTIAL

There is presently a major experimental and theoretical thrust[45] toward generating spin-polarized quantum liquids and understanding their properties. An important step in the experimental effort is to construct samples that minimize spin-flip transitions.[46] For that purpose, chambers are used with walls covered by ^{4}He. Thus it is of interest to study the interaction between a helium film covering a wall and an impurity atom.

Systems of ^{3}He atoms adsorbed on the free surface[47] or to films of liquid ^{4}He are also of independent special interest.[48–50] This system is an (almost) ideal two-dimensional Fermi liquid; a layer of ^{3}He atoms with a density less than that of a monolayer may be considered as an impurity model. On the surface of bulk ^{4}He, the impurity particles have a binding energy[46,51] of about 2.2 K relative to the state where the ^{3}He atom lives in bulk ^{4}He. The physical picture becomes more complicated for the case of ^{3}He atoms on films of ^{4}He. A second "layered" state may exist within the medium,[52] which generates a mixture of a quasi-two-dimensional and a three-dimensional system. The ability to change the properties of the ^{3}He with the thickness of the ^{4}He background makes these systems experimentally very interesting,[53] and poses a challenging theoretical problem.

Studies of the interaction between a homogeneous or inhomogeneous helium liquid and an impurity atom are abundant.[9,36,54–60] The reconsideration of this problem is required by the better wave function available through the present work. We recall also the special experimental interest in our specific physical model which explicitly takes into account the presence of the substrate and the layer structure. We will see that the layer structure of the density leads to an average field that is significantly different from semimicroscopic approaches[33,49,50] used recently to study the same problem.

If the impurity atom is of a different species (for example, hydrogen), one must introduce two different kinds of two-body correlations,[36,58–60] and essentially repeat the optimization procedure described here for the helium-impurity correlations. The numerical application of this aspect of our theory is in progress.[61]

The problem is much simpler for the case of a ^{3}He impurity atom. Since the ^{4}He-^{4}He and the ^{4}He-^{3}He interactions are the same, it is reasonable to assume[9,54,56,57] that the two-body correlation factor $u_2(\mathbf{r}_i,\mathbf{r}_j)$ is independent of the species. We may therefore use for the $A+1$ particle system, consisting of one ^{3}He atom and A ^{4}He atoms, the wave function[54]

$$\Psi_0(\mathbf{r}_0,\mathbf{r}_1,\ldots,\mathbf{r}_A) = \exp\left[\tfrac{1}{2}u_1^{(3)}(\mathbf{r}_0)+\tfrac{1}{2}\sum_{i=1}^{A}u_1(\mathbf{r}_i)+\tfrac{1}{2}\sum_{\substack{i,j=0\\ i<j}}^{A}u_2(\mathbf{r}_i,\mathbf{r}_j)\right] . \tag{6.1}$$

A second reason that the wave function (6.1) is sufficient for calculating the binding energy of a ^{3}He impurity is that usually binding energies depend only weakly on the two-body correlations as long as these are within reasonable bounds. A third reason will become apparent below, where we will show that the contribution from two-body correlations to the average field seen by the impurity atom is weak and quite structureless.

Using the simple *ansatz* (6.1) for the many-body wave function, Lekner[54] minimized the total energy with respect to the one-body correlation $u_1^{(3)}(\mathbf{r})$ to obtain a one-body Schrödinger equation for the impurity wave function

$$-\frac{\hbar^2}{2m_3}\nabla^2\psi(\mathbf{r})+U(\mathbf{r})\psi(\mathbf{r})=\epsilon\psi(\mathbf{r}) , \tag{6.2}$$

with

$$\psi(\mathbf{r})=[\rho_1(\mathbf{r})]^{1/2}\exp\{[u_1^{(3)}(\mathbf{r})-u_1(\mathbf{r})]/2\} , \tag{6.3}$$

and

$$U(\mathbf{r})=-\frac{\hbar^2}{2m_3}\frac{\nabla^2[\rho_1(\mathbf{r})]^{1/2}}{[\rho_1(\mathbf{r})]^{1/2}}+\left[\frac{m_4}{m_3}-1\right]W(\mathbf{r}) ,$$
$$W(\mathbf{r})=\frac{A+1}{\rho_1(\mathbf{r})}\int d^3r_1\int d^3r_2\cdots\int d^3r_A\,\Psi_0(\mathbf{r},\mathbf{r}_1,\mathbf{r}_2,\ldots,\mathbf{r}_A)\left[-\frac{\hbar^2}{2m_4}\nabla_r^2\right]\Psi_0(\mathbf{r},\mathbf{r}_1,\mathbf{r}_2,\ldots,\mathbf{r}_A) . \tag{6.4}$$

Equations (6.4) are more general in the sense that they also hold if species-independent multiparticle correlations are present. The eigenvalue ϵ of Eq. (6.2) is the difference in energy between an $(A+1)$-particle system of ^{4}He atoms and a system of A ^{4}He atoms *plus* one ^{3}He atom. In the special case of one- and two-body correlations, the potential $W(\mathbf{r})$ is given explicitly in terms of the known ingredients of the variational theory:[56]

$$W(\mathbf{r}_1)=-\frac{\hbar^2}{8m_4}\left[\rho_1^{-1}(\mathbf{r}_1)\nabla^2\rho_1(\mathbf{r}_1)+\nabla^2u_1(\mathbf{r}_1)+\int d^3r_2\,\rho_1(\mathbf{r}_2)g(\mathbf{r}_1,\mathbf{r}_2)\nabla_{\mathbf{r}_1}^2u_2(\mathbf{r}_1,\mathbf{r}_2)\right] . \tag{6.5}$$

As usual, it is convenient to eliminate the correlation functions $u_1(\mathbf{r}_1)$ and $u_2(\mathbf{r}_1,\mathbf{r}_2)$ in favor of the one-body density, the pair distribution function, and the other compound-diagrammatic quantities of the HNC theory. Doing this, we arrive at the HNC approximation for the impurity potential,

$$U(\mathbf{r}_1)=\frac{\hbar^2}{2m_4}\frac{\nabla^2[\rho_1(\mathbf{r}_1)]^{1/2}}{[\rho_1(\mathbf{r}_1)]^{1/2}}+\left[\frac{\hbar^2}{2m_4}-\frac{\hbar^2}{2m_3}\right]\int d^3r_2\,\rho_1(\mathbf{r}_2)\{\,|\,\nabla_{\mathbf{r}_1}[g(\mathbf{r}_1,\mathbf{r}_2)\,|\,^2]^{1/2}-\tfrac{1}{4}\nabla_{\mathbf{r}}g(\mathbf{r}_1,\mathbf{r}_2)\cdot\nabla_{\mathbf{r}}N(\mathbf{r}_1,\mathbf{r}_2)\}\ . \quad (6.6)$$

In order to estimate the importance of the different terms in the mean-field equation (6.2), we compare in Fig. 13 the full mean field $U(z)$, the substrate potential $U_{\rm sub}(z)$, and the term $(\hbar^2/2m_4)\rho_1^{-1/2}(\mathbf{r})\nabla^2\rho_1^{1/2}(\mathbf{r})$ for the thickest film in the medium strength substrate potential model II. Models I and III, respectively, show weaker and stronger fluctuations. The one-body potential has been extrapolated smoothly to its asymptotic value $-\mu$, since the variational ground-state calculations become numerically inaccurate below a few percent of the maximum density. We found, in agreement with Ref. 56, that the strongly bound eigenstates of Eq. (6.2) depend very weakly on the asymptotic details of the one-body potential. The uncertainty in the higher-lying states is somewhat larger; the energies depend somewhat on how the extrapolation to the asymptotic value is done. From numerical tests we concluded that the third state is accurate within about 10%.

Most of the structure of the one-body potential is obviously due to the structure of $\rho_1^{-1/2}(\mathbf{r})\nabla^2\rho_1^{1/2}(\mathbf{r})$ which, in turn, is induced by the layer structure of the one-body density. This finding lends credibility to the Lekner approximation: One should expect that this approximation becomes worse with increasing density. But the approximation enters only second term in Eq. (6.6), whereas the first term becomes the dominating one in the first two or three layers. We regard therefore the Lekner approximation for the impurity wave function as adequate. The potential is characterized by its broad minimum close to the free surface, and by one or more sharper minima in phase with the layers of the density profile. Depending on the balance between potential and kinetic energy, one should expect at least two bound states, one close to the surface, and another one in the deepest of the secondary potential minima.

Our solutions of the eigenvalue problem (6.2) confirm this expectation; the three models under consideration cover a broad range of the possibilities. Figures 14–16 show the occupation probabilities $\delta\rho_1^{(3)}(\mathbf{r})=|\,\Psi(\mathbf{r})\,|^2$ of the ^{3}He impurity for the thickest films in the three potential models I–III. In all three cases, we find that the lowest state is localized in the surface by the broad minimum of the potential there.

The second bound state of the impurity atom is localized more toward the substrate boundary, but the degree of localization and its position depend on the strength of the potential wells, and hence on the local density. In the strongest potential, the second state is located at about the third atomic layer. The impurity does not penetrate into the very high-density regimes of the first two layers, in which the liquid model is only a crude approximation. We have argued above that only the first monolayer of model II should be solid. We see (cf. Fig. 15) that the second bound state in that model can partly penetrate the third layer, but still has a very small occupation probability inside the first layer. Finally, in the weak potential model III, the second bound state is mostly localized within the first atomic layer. The density of that layer is sufficiently low that a liquid model is adequate. We conclude from this that the second bound state will penetrate into the system up to a certain maximum density. There is no *a priori* reason that this density is related to the soli-

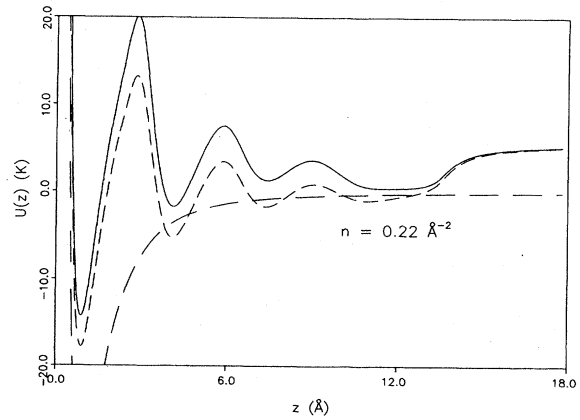

FIG. 13. The effective potential seen by a ^{3}He impurity is shown for the potential model II, and the film with a particle number $n=0.22$ Å^{-2} (solid line). Also shown is the bare substrate potential (long-dashed line) and the term $(\hbar^2/2m_4)\rho_1^{-1/2}(\mathbf{r})\nabla^2\rho_1^{1/2}(\mathbf{r})$ (short-dashed line).

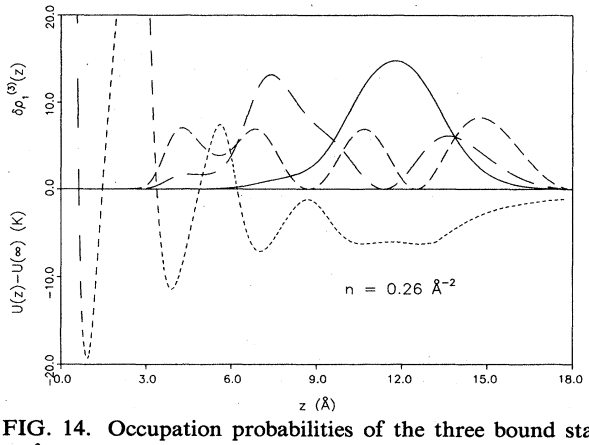

FIG. 14. Occupation probabilities of the three bound states of a ^{3}He impurity (solid, long-dashed, and short-dashed lines with increasing energy) are shown for the film with $n=0.26$ Å^{-2} in the strong substrate potential model I. Also shown is, for comparison, the impurity potential (short-dashed line in the lower half of the figure). The normalization of the occupation probability, $\delta\rho_1^{(3)}(z)=|\,\Psi(z)\,|^2$, is arbitrary.

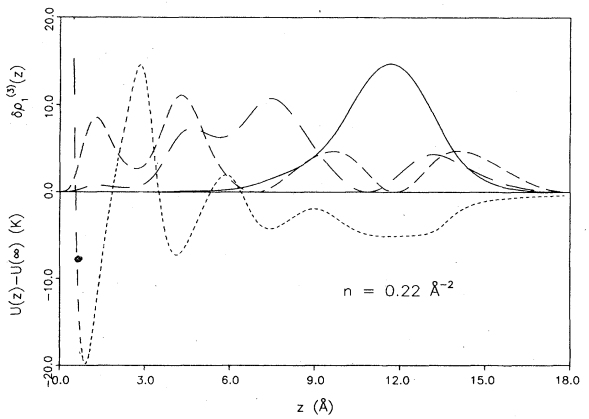

FIG. 15. Same as Fig. 14 in the potential model II for $n=0.22$ Å^{-2}.

dification density of a monolayer. But it is reassuring that the model does not have the unphysical feature of predicting the penetration of the impurity into a solid layer of high density.

The third state looks very much like that of a free particle confined in a box of the size of the film, being only little affected by the details of the one-body potential. (Note that this state does not appear in the very thin films of model III.) The only qualitative difference in model I is that this third state can penetrate the second atomic layer. It is not clear to what extent this possibility is an artifact of our assumption of a liquid state throughout the film. It seems plausible to identify the third state with the lower bound of a set of continuum states which should appear as the thickness of the film is increased. These continuum states correspond to ^{3}He particles of finite momentum that live in bulk ^{4}He.

This interpretation is confirmed by considering the eigenvalues of Eq. (6.2), which are given in Tables IV–VI. The third eigenvalue (note that the chemical potential μ must be added to obtain the energy compared with a particle of energy zero at infinity) is close to the binding energy of a ^{3}He impurity in bulk ^{4}He. To interpret the difference between our eigenstate and the bound state of an impurity in the bulk fluid, the reader is reminded of the different physical situation: The impurity particle is here confined to a box only five times its size, which should increase its zero-point energy. On the other hand, additional binding comes from the attractive substrate potential. A comparison of the dependence of μ (Tables I–III) on the film thickness in the three models under consideration should give an adequate estimate of that effect.

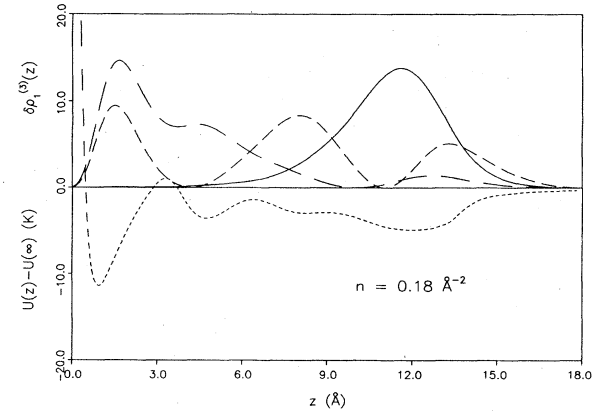

FIG. 16. Same as Fig. 14 in the weak potential model III for $n=0.18$ Å^{-2}.

TABLE IV. The bound states of a ^{3}He atom in the ^{4}He films in the strong substrate potential model I.

n (Å^{-2})	ϵ_2 (K)	ϵ_2 (K)	ϵ_3 (K)
0.14	2.83	5.83	7.66
0.16	2.14	4.60	7.89
0.18	1.99	4.61	6.58
0.20	1.94	4.27	5.51
0.22	1.79	3.90	5.45
0.24	1.71	3.75	5.28
0.26	1.64	3.57	4.98

Our results are in good agreement with the ones of Refs. 9 and 56; taking this interpretation of the *third* eigenstate as the continuum boundary for impurities in the bulk, we obtain approximately 2.4 K for the energy of the bound state in the surface for model III. This is in good agreement with the experimental value[47,51] of 2.22 K. The weak-potential model III, corresponds most closely to a bulk system.

Interesting implications follow from our result for the problem of dilute layers of ^{3}He atoms in films of ^{4}He. In particular, we find two locations where a two-dimensional layer can form. This second state has not been found in comparable recent work[33,49,50] which assumes a simpler structure in the one-body density. The existence of such a second state is in agreement with experimental evidence[48] and theoretical predictions.[52] We hesitate, as discussed above, to identify the third excited state with a localized one that would be needed to give indication for additional layered substructures. This is not in contradiction to experiment: DiPirro and Gasparini[48] point out that specific-heat data can equally well be fitted with a three-dimensional model of the ^{3}He component. It also seems plausible that the second state contributes little to specific heat data in thick films, since the overlap with the surface state decreases with the thickness of the film.

TABLE V. The bound states of a ^{3}He atom in the ^{4}He films in the medium strength substrate potential model II.

n (Å^{-2})	ϵ_1 (K)	ϵ_2 (K)	ϵ_3 (K)
0.12	1.93	4.06	5.10
0.14	1.71	3.66	5.06
0.16	1.66	3.56	4.86
0.18	1.62	3.38	4.55
0.20	1.56	3.24	4.41
0.22	1.55	3.17	4.25

TABLE VI. The bound states of a ^{3}He atom in the ^{4}He films in the weak substrate potential model III. There is no third bound state below $n=0.12$ Å^{-2}.

n (Å^{-2})	ϵ_1 (K)	ϵ_2 (K)	ϵ_3 (K)
0.08	1.76	3.44	
0.10	1.88	3.37	
0.12	1.92	3.30	5.15
0.14	1.97	3.32	4.87
0.16	1.97	3.32	4.62
0.18	1.99	3.34	4.44

Our results for the energy difference $\Delta\epsilon=\epsilon_3-\epsilon_1$ agree qualitatively with those of Refs. 33, 49, and 50. Differences may be attributed to different substrate models. References 33, 49, and 50 consider ^{4}He on Nuclepore filters, whose van der Waals interactions are about halfway between models I and II in strength. The reader is also reminded that no information on macroscopic properties of bulk ^{4}He or on ^{4}He films went into our calculation. This restricts the accuracy of the predictions to the general accuracy of the HNC theory of bulk ^{4}He.

VII. SUMMARY

Let us briefly discuss the achievements and implications of the theory that was derived in I and II and applied and extended here. As far as the calculation of ground-state properties are concerned, we have achieved the best that can be done within the restrictions of one- and two-body correlations and the HNC approximation. The accuracy with which we could predict ground-state properties is consistent with what we found in I and with the general uncertainties of the HNC approximation. "Better" agreement of earlier work[9–12] with experimental surface tensions is a consequence of additional approximations such as local-density approximation or parametrized correlation functions, not due to a better microscopic theory. To improve upon the microscopic description, elementary diagrams and three-body correlations must be included[27] or fitted to known Monte Carlo data or experiments.

Surface energies, and consequently the dispersion relation of the collective modes, should be most strongly affected by an improvement of the ground-state description. But we believe that the layer structure, which is characteristic for a film on a substrate, is described correctly in both amplitude and wavelength.

We have commented separately on the credibility of the HNC theory of the density matrix. We believe that the results presented in Sec. V are within the typical accuracy of the HNC theory, i.e., within about 20%. The impurity states discussed in Sec. VI are probably the quantities described best within the present theory, since the dominant part of the impurity potential does not depend on the main uncertainty of the theory, i.e., the saturation density.

The most important achievement of this series of papers is the demonstration that the optimization problem can be solved efficiently, and that the solutions can be interpreted physically and used for further applications. As in I, the computational effort is reasonable and leaves room for further refinements: depending on the thickness of the film, one iteration of the complete PPA procedure takes between 10 and 40 min on a VAX 780 computer. About ten iterations are needed to reach convergence.

Further application of the methods developed here are foreseen. One of the most immediate goals is a more general impurity theory;[61] another field of interest could be the study of interfaces. It is quite straightforward to derive an impurity-impurity interaction in the sense of Ref. 62. But we believe that a quantitative treatment of the properties of two-dimensional layers of ^{3}He atoms requires the inclusion of momentum-dependent correlations, either in the trial wave function,[63] or in a perturbative way within the method of correlated basis functions.[2]

ACKNOWLEDGMENTS

This work was supported by the Deutsche Forschungsgemeinschaft. Warm hospitality and support at the Max-Planck-Institut für Kernphysik in Heidelberg, where most of this work was performed, is gratefully acknowledged. I would also like to thank Dr. D. O. Edwards, Dr. J. DuPont-Roc, and Dr. F. M. Gasparini for comments on an earlier version of this paper, and R. A. Smith for a critical reading of the manuscript.

*Present address.
[1]E. Krotscheck, G.-X. Qian, and W. Kohn, Phys. Rev. B **31**, 4245 (1985).
[2]E. Feenberg, *Theory of Quantum Liquids* (Academic, New York, 1969).
[3]C.-W. Woo, in *Physics of Liquid and Solid Helium,* edited by K. H. Bennemann and J. B. Ketterson (Wiley, New York, 1976), Vol. 1; C. E. Campbell, in *Progress in Liquid Physics,* edited by C. A. Croxton (Wiley, London, 1977), Chap. 6.
[4]M. H. Kalos, M. A. Lee, P. A. Whitlock, and G. Chester, Phys. Rev. B **24**, 115 (1981).
[5]C. E. Campbell and E. Feenberg, Phys. Rev. **188**, 396 (1969).
[6]L. J. Lantto and P. J. Siemens, Phys. Lett. **68B**, 308 (1977).
[7]E. Krotscheck, Phys. Rev. A **15**, 397 (1977).
[8]L. Castillejo, A. D. Jackson, B. K. Jennings, and R. A. Smith, Phys. Rev. B **20**, 3631 (1979).
[9]Y. M. Shih and C.-W. Woo, Phys. Rev. Lett. **30**, 478 (1973).
[10]F. D. Mackie and C.-W. Woo, Phys. Rev. B **18**, 529 (1978).
[11]C. C. Chang and M. Cohen, Phys. Rev. A **8**, 1930 (1973).
[12]M. Saarela, P. Pietiläinen, and A. Kallio, Phys. Rev. B **27**, 231 (1983).
[13]E. Krotscheck, Phys. Rev. B **31**, 4258 (1985).
[14]L. Reatto and G. V. Chester, Phys. Rev. **155**, 88 (1967).
[15]C. E. Campbell, K. E. Kürten, M. L. Ristig, and G. Senger, Phys. Rev. B **30**, 3728 (1985).
[16]R. O. Hilleke, P. Chaddah, R. O. Simmons, D. L. Price, and

S. K. Sinha, Phys. Rev. Lett. **52**, 847 (1984).
[17]M. L. Ristig and J. W. Clark, Phys. Rev. B **14**, 2875 (1976).
[18]S. Fantoni, Nuovo Cimento **44A**, 191 (1978).
[19]R. A. Aziz, V. P. S. Nain, J. C. Carley, W. L. Taylor, and G. T. McConville, J. Chem. Phys. **70**, 4330 (1979).
[20]R. Siddon and M. Schick, Phys. Rev. A **9**, 907 (1974); **9**, 1753 (1974).
[21]F. Ricca, Nuovo Cimento Suppl. **5**, 339 (1967).
[22]M. W. Cole, D. R. Frankl, and D. L. Goodstein, Rev. Mod. Phys. **53**, 199 (1981).
[23]A. D. Novaco and C. E. Campbell, Phys. Rev. B **11**, 2525 (1975); A. D. Novaco, *ibid.* **13**, 3194 (1976).
[24]A. D. McLachlan, Mol. Phys. **7**, 381 (1964).
[25]G. Vidali and M. W. Cole, Phys. Rev. B **22**, 4661 (1980).
[26]J. DuPont-Roc (private communication).
[27]C. C. Chang and C. E. Campbell, Phys. Rev. B **15**, 4238 (1977).
[28]J. G. Dash and M. Schick, in *Physics of Liquid and Solid Helium,* edited by K. H. Bennemann and J. B. Ketterson (Wiley, New York, 1976), Vol. 2.
[29]M. Bretz, in *Monolayer and Submonolayer Helium Films,* edited by J. G. Daunt and E. Lerner (Plenum, New York, 1973), p. 11.
[30]A. D. Jackson, B. K. Jennings, A. Lande, and R. A. Smith, Phys. Rev. B **24**, 105 (1981).
[31]E. Krotscheck and R. A. Smith (unpublished).
[32]R. L. Eglin and L. Goodstein, Phys. Rev. A **9**, 2657 (1974).
[33]D. S. Sherill and D. O. Edwards, Phys. Rev. B **31**, 1338 (1985).
[34]C. C. Chang and M. Cohen, Phys. Rev. B **11**, 1059 (1974).
[35]C.-W. Woo (private communication to C. E. Campbell, 1974).
[36]R. A. Guyer, M. D. Miller, and J. Yaple, Phys. Rev. B **25**, 4570 (1982).
[37]C. N. Yang, Rev. Mod. Phys. **34**, 694 (1962).
[38]J. H. Scholtz, E. O. McLear, and I. Rudnik, Phys. Rev. Lett. **32**, 147 (1974); M. H. W. Chan, A. W. Yanof, and J. D. Reppy, *ibid.* **32**, 1347 (1974).
[39]E. Feenberg (private communication to J. W. Clark and M. L. Ristig, 1975).
[40]D. Ruelle, *Lecture Notes of the Theoretical Physics Institute* (University of Colorado Press, Boulder, 1963); D. Ruelle, Rev. Mod. Phys. **36**, 580 (1964).
[41]M. L. Ristig, P. M. Lam, and J. W. Clark, Phys. Lett. **55A**, 101 (1975); P. M. Lam and C. C. Chang, *ibid.* **59A**, 356 (1976).
[42]A. D. Jackson, A. Lande, and R. A. Smith, Phys. Rep. **86**, 55 (1982).
[43]M. F. Flynn, J. W. Clark, R. M. Panoff, O. Bohigas and S. Strignari, Nucl. Phys. **427A**, 253 (1984).
[44]M. Puoskari and A. Kallio, Phys. Rev. B **30**, 152 (1984).
[45]C. Lhuillier and D. Levesque, Phys. Rev. B **23**, 2203 (1981); H. R. Glyde and S. I. Hernadi, in *Quantum Fluids and Solids—1983 (Sanibel, Florida),* edited by E. D. Adams and G. G. Ihas (AIP, New York, 1983); E. Krotscheck, J. W. Clark, and A. D. Jackson, Phys. Rev. B **28**, 5088 (1983).
[46]I. F. Silvera and J. T. M. Walraven, Phys. Rev. Lett. **44**, 164 (1980).
[47]D. O. Edwards and W. F. Saam, in *Progress in Low Temperature Physics,* edited by D. F. Brewer (North-Holland, New York, 1978), Vol. 7A, p. 282.
[48]M. J. DiPirro and F. M. Gasparini, Phys. Rev. Lett. **44**, 269 (1980); B. Bhattacharyya and F. M. Gasparini, *ibid.* **49**, 919 (1982).
[49]F. M. Gasparini, B. Bhattacharyya, and M. J. DiPirro, Phys. Rev. B **29**, 4921 (1984).
[50]D. S. Sherill and D. O. Edwards, in Proceedings of the XVII International Conference on Low Temperature Physics, Karlsruhe, West Germany (1984) (unpublished).
[51]H. M. Guo, D. O. Edwards, E. Sarwinski, and J. T. Tough, Phys. Rev. Lett. **27**, 1259 (1971).
[52]K. K. Mon and W. F. Saam, Phys. Rev. B **23**, 5824 (1981).
[53]B. Bhattacharyya, M. J. DiPirro, and F. M. Gasparini, Phys. Rev. B **31**, 2719 (1985).
[54]J. Lekner, Philos. Mag. **22**, 669 (1970).
[55]W. F. Saam, Phys. Rev. A **4**, 1278 (1971).
[56]C. C. Chang and M. Cohen, Phys. Rev. B **8**, 3131 (1973).
[57]R. A. Guyer and M. D. Miller, Phys. Rev. Lett. **47**, 349 (1981).
[58]J. Owen, Phys. Rev. Lett. **47**, 586 (1981).
[59]K. E. Kürten and M. L. Ristig, Phys. Rev. B **27**, 5479 (1983).
[60]A. Kallio, P. Pietiläinen, and L. J. Lantto, Phys. Scr. **25**, 943 (1982); P. Pietiläinen and A. Kallio, Phys. Rev. B **27**, 224 (1983).
[61]M. L. Ristig (private communication).
[62]D. O. Edwards, J. D. Feder, and V. U. Nayak, in *Quantum Fluids and Solids,* edited by S. B. Trickey, E. D. Adams, and J. W. Duffy (Plenum, New York, 1977) p. 375.
[63]J. Owen, Phys. Rev. B **23**, 5815 (1981).